ALUMINUM K X-RAY PRODUCTION AND ELECTRON

TRANSFER CROSS SECTIONS FOR OXYGEN, NITROGEN, AND FLUORINE

IONS FROM 0.6 TO 2.2 MEV/AMU

by

Glenn S. Gealy

B. A., Hastings College, 1974
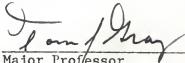

A MASTER'S THESIS

submitted in partial fulfillment of the

requirements for the degree

MASTER OF SCIENCE

Department of Physics

Kansas State University

Manhattan, Kansas 66506

1978

Approved by:

_____

Major Professor

TABLE OF CONTENTS

i

LIST OF FIGURES

ACKNOWLEDGEMENTS

I. INTRODUCTION

With the discovery of x-rays by Roentgen just prior to 1900 began the study of inner-shell atomic processes. As early as 1912 Chadwick[1] was experimenting with alpha particle-induced inner-shell ionization, the forerunner of similar experiments done today. The invention of linear accelerators in the 1930's gave physicists a tool for more comprehensive studies of ion-atom collisions, and considerable interest has been focused on inner-shell vacancy production in such systems. With the advent of the non-dispersive Si(Li) x-ray detector came the furthering of interests in inner-shell ionization processes for heavy ions incident upon a variety of targets.[2]

Detection of characteristic x-ray or energetic electron (Auger) emission from the decay of excited atoms, in the case of K-shell ionization, has given the physicist a means of evaluating theoretical models of the K-shell ionization process. When an energetic projectile passes in the vicinity of the target atom, several different target K-shell ionization processes are possible. These processes depend on the atomic numbers Z_1 and Z_2, projectile velocity, violence of the collision or impact parameter, and atomic states of the collision partners. Stationary states of the target atom are perturbed by the projectile so that target K-shell electrons may be a) ionized to the target continuum, which is referred to as direct Coulomb ionization, b) transferred into vacant bound projectile states, c) ionized to the projectile continuum, or d) excited to higher bound target states. In any case the result is the creation of a target K-shell vacancy which is filled by decay resulting in K-shell x-ray or Auger electron emission. The probability of de-excitation by x-ray emission is determined by the

1

K-shell fluorescence yield, which is dependent upon the electronic configuration.

Where K-shell ionization by light ions, $Z_1 < 3$, has been concerned, theoretical treatment of direct Coulomb ionization has been limited to bare point charges where $Z_1/Z_2 << 1$. The three most prominent approximations in this regard are the classical impulse or binary encounter approximation (BEA)[3], semiclassical approximation (SCA)[4], and the quantum mechanical plane wave Born approximation (PWBA)[5].

In the BEA, the ionization process is viewed as a two body interaction between the projectile with velocity v_1 and the target electron with average orbital velocity v_{2K}. The presence of the target nucleus and other electrons is relevant only to the extent that they serve to define the velocity distribution and binding energy of the target electron.

In the SCA the projectile is treated as a classical particle with a well defined trajectory. This requires that the projectile wave packet is small compared to the distance of closest approach to the nucleus. The K-shell direct Coulomb ionization cross section $\sigma_{K(DC)(SCA)}$ is calculated in the classical manner

$$\sigma_{K(DC)(SCA)} = \int_0^\infty 2\pi b \ db \ P_K(b)$$

where $P_K(b)$ is the impact parameter-dependent probability of K-shell ionization.

The PWBA treats the projectile as a plane wave with incoming and outgoing wave vectors differing vectorially by an amount of momentum transferred to the electron. The quantum mechanical direct Coulomb ionization cross section $\sigma_{K(DC)(PWBA)}$ is proportional to the square of the transition matrix element, $|T_{if}|^2$, where

2

$$|T_{if}| = <f|V|i> \quad .$$

Here, V is given by the Coulomb potential between the projectile nucleus and target electron, $-z_1 e^2/|\vec{r}_1 - \vec{r}_2|$, where $\vec{r}_1$ is $\vec{r}_{projectile}$ and $\vec{r}_2$ is $\vec{r}_{electron}$. The initial and final wave functions $|i>$ and $<f|$ are taken to be the products of the incoming plane wave times the target ground state wave function, and the outgoing plane wave times the final target state (continuum) wave function, respectively. From the form of T_{if} it can be seen immediately that $\sigma_{K(DC)(PWBA)}$ is proportional to z_1^2, since

$$|T_{if}|^2 = z_1^2 |<f|(e^2/|\vec{r}_1 - \vec{r}_2|)|i>|^2 \quad . \qquad \text{eq. I. 1}$$

This z_1^2 scaling is also basic to both the BEA and SCA.

For ^{1,2}H and ^{3,4}He projectiles incident on a variety of targets, the reduced PWBA K-shell ionization cross sections fit experimental data reasonably well at higher scale velocities, v_1/v_{2K}, as shown in Fig. 1(a) from Ref. 2. However as v_1/v_{2K} decreases the agreement between theory and data deteriorates, and experimental values of the cross section are over-predicted by factors of ≤ 30. To account for these discrepancies several authors[4,6-9] have included corrections to the PWBA which have found varying degrees of success. Basbas, Brandt, and Laubert (BBL)[7,9] incorporate the effects of Coulomb deflection and increased target K-shell binding energy into the PWBA. These considerations introduce z_1^3 and additional z_2, M_1, M_2, and v_1 effects which bring experiment and theory into good agreement for light ions as shown in Fig. 1(b) from Ref. 2. Their most recent paper[9] also includes the effects of target K-shell polarization.

The theories of BBL, referred to as PSS, and additional effects that represent contributions due to electron transfer from the target

3

FIGURE 1

(a) Universal PWBA direct Coulomb ionization cross sections for light ions on a variety of targets from Ref. 2.

(b) Universal PSS(CB) direct Coulomb ionization cross sections for light ions on a variety of targets from Ref. 2.

5
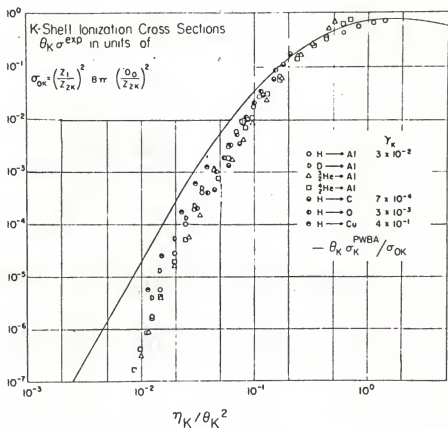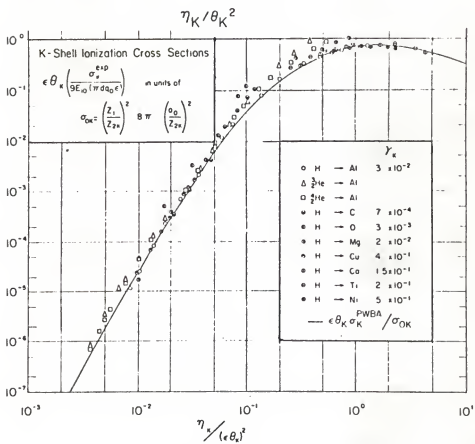
to the projectile, target thickness effects, and fluorescence yields, as they relate to the K-shell ionization of ^{27}Al by ^{14}N^{+q}, ^{16}O^{+q}, and ^{19}F^{+q} projectiles will be discussed in Sec. II. The last three areas mentioned above are very critical in the interpretation of target K x-ray production data where the projectiles are heavy ions, i.e. C, N, O, ect. A description of the experimental Al K x-ray production cross section measurements are given in Sec. III, and the results are analyzed and compared to theoretical calculations in Sec. IV. A summary is given in Sec. V.

II. THEORY

In this chapter, the theoretical foundations of K-shell ionization and target K x-ray production data interpretation for incident heavy ions are presented. The discussion is developed for direct Coulomb ionization, i.e. the PSS theories of BBL, electron transfer, target thickness effects, and fluorescence yields.

A. PSS Model

As its name implies, PSS, or Perturbed Stationary State theory includes consideration of the perturbation of stationary atomic states by the projectile in calculation of target K-shell ionization cross sections. In the initial work of BBL[7], henceforth referred to as PSS(CB), the PWBA cross sections are reduced by inclusion of a Coulomb deflection correction (C) resulting from the hyperbolic rather than straight line path of a classical projectile due to the repulsion between projectile and target nucleii. In addition a perturbation due to the presence of the projectile charge which is manifested as a Z_1^3-dependent increase in effective target K-shell binding energy (B) also serves to reduce the ionization cross section. The most recent theory[9] will be referred to as NPSS(CBP), N for "new". In addition to the B and C corrections of PSS(CB), the NPSS(CB) calculations include the effect of target K-shell polarization by the projectile (P). This serves to decrease the effective target K-shell binding energy by increasing the average unperturbed K-shell radius $<r_K>$ and thus introduces an additive Z_1^3 effect. An additional basic difference between PSS(CB) and NPSS(CBP) is the following: PSS(CB) assumes that projectiles at all impact parameters contribute to the binding correction B, whereas NPSS(CBP) specifies that only projectiles for which

7

$$b \leq c_K \, a_{OK} = c_K \langle r_K \rangle / 1.5$$

effect B. Furthermore, NPSS(CBP) assumes that contributions to P are limited to projectiles with

$$b > c_K \, a_{OK} \quad .$$

It is suggested[9] that $c_K = 1.5$.

The relationship of the PWBA, PSS(CB), and NPSS(CBP) K-shell ionization cross sections can be seen by comparison of the explicit expressions[7,9]

$$\sigma_{K(DC)(PWBA)} = \sigma_{OK} F_K(\eta_K/\theta_K^2)/\theta_K \quad , \qquad \text{eq.II.A.1}$$

$$\sigma_{K(DC)(PSS(CB))} = 9E_{10}(\pi d q_o \varepsilon)(\sigma_{OK}/\varepsilon\theta_K) F_K(\eta_K/\varepsilon^2\theta_K^2), \quad \text{eq.II.A.2}$$

$$\sigma_{K(DC)(NPSS(CBP))} = 9E_{10}(\pi d q_o \zeta_K)(\sigma_{OK}/\zeta_K\theta_K) F_K(\eta_K/\zeta_K^2\theta_K^2). \quad \text{eq.II.A.3}$$

The $9E_{10}(y)$ factor is the Coulomb deflection correction to the PWBA, with $\varepsilon\theta_K$ and $\zeta_K\theta_K$ specifying the net modifications to the observed dimensionless K-shell binding energy θ_K. Relevant quantities for these calculations are defined below:

$$\sigma_{OK} = 8\pi(a_0/Z_{2K})^2(Z_1/Z_{2K})^2 = 8\pi a_0^2(Z_1/Z_{2K}^2)^2,$$

θ_K = (observed target K-shell binding energy/screened

hydrogenic K-shell binding energy) = $\hbar\omega_{2K}/Z_{2K}^2 13.6$ eV,

$$\eta_K = (v_1/v_{2K})^2 = (E_1/M_1)/1836 \, Z_{2K}^2 13.6 \text{ eV},$$

$$9E_{10}(y) \cong 9e^{-y}/(9 + y),$$

with $d = Z_1 Z_2 \, e^2/Mv_1^2,$

$$q_o = \omega_{2K}/v_1 \, ,$$

$$1/M = 1/M_1 + 1/M_2 \quad .$$

8

$$a_o = \hbar^2/e^2 m_e = 5.29 \times 10^{-9} \text{cm},$$

$$Z_{2K} = Z_2 - 0.3,$$

$$\xi_K = 2\eta_K^{1/2}/\theta_K \;,$$

$$\epsilon = 1 + 2(Z_1/Z_{2K}\theta_K)\; g(\xi_K) \text{ with } g(x) = (1 + x)^{-5}(1 + 5x$$
$$+ 7.14x^2 + 4.27x^3 + 0.947x^4),$$

$$\zeta_K = 1 + (2Z_1/\theta_K Z_{2K})(g(\xi_K, c_K) - h(\xi_K, c_K))$$

with $g(\xi_K, c_K)$ given by interpolation from Table IV
or Eqs. (39) – (42), Ref. 9, and with

$$h(\xi_K, c_K) = (2/\theta_K \xi_K^3)(I(c_K/\xi_K)), \text{ where}$$

$$I(x) = \begin{cases} (3\pi/4)(\ln(1/x^2) - 1), \text{ for } 0 < x \leq 0.035, \\ e^{-2x}(0.031 + 0.21x^{1/2} + 0.005x - 0.069x^{3/2} + \\ \quad 0.324x^2)^{-1}, \text{ for } 0.035 < x \leq 3.1, \text{ or} \\ 7 \times 10^{-4} \approx 0, \text{ for } x > 3.1 \end{cases}$$

or by interpolation from Table IV, Ref. 9.

F(y) can be obtained from Table V, Ref. 7 by interpolation, or can be taken from extended tables calculated by Rice, Basbas, and McDaniel[10].

Consideration of ϵ and ζ_K shows that $g(\xi_K)$ and $g(\xi_K, c_K)$ are the increased binding energy functions for PSS(CB) and NPSS(CBP) calculations, respectively. As one would expect, $g(\xi_K, c_K = \infty)$ is equivalent to $g(\xi_K)$ since both would then include all impact parameters, $b = 0$ to $b = \infty$, in the binding energy correction. $I(x)$ is the polarization correction function, from Ref. 9. The functions I and g introduce Z_1^3 effects into the ionization calculations. $I(c_K/\xi_K)$ decreases as c_K increases so that by setting c_K very large, the polarization correction

9

vanishes. It should also be noted that by calculating

$$\zeta_K = \zeta_K \; (g(\xi_K, \infty) - h(\xi_K, 1.5))$$

the NPSS(CBP) calculations reduce to PSS(CBP). At low values of v_1/v_{2K} Coulomb deflection and increased binding effects are maximized, while polarization effects are larger at higher v_1/v_{2K} values.

The term "reduced cross section" is applied to the expression

$$F_K(\eta_K/\zeta_K^2\theta_K^2) = \sigma_{K(DC)(NPSS(CBP))}\zeta_K\theta_K/9E_{10}(\pi dq_o\zeta_K)\sigma_{OK} \quad .$$

Upon plotting $F_K(\eta_K/\zeta_K^2\theta_K^2)$ vs $\eta_K/\zeta_K^2\theta_K^2$, a universal form for the ionization of the target K-shell is obtained. The results of PWBA, PSS(CB), PSS(CBP), NPSS(CB), and NPSS(CBP) K-shell direct Coulomb ionization cross sections for O ions on Al are shown in Fig. 2. The introduction of radial cutoffs into the calculation of the binding energy correction effect results in an increase of the calculated cross section by a factor of $\simeq 3$, i.e.,

$$\sigma_{K(DC)(NPSS(CB))}/\sigma_{K(DC)(PSS(CB))} \simeq 3 \quad .$$

B. Electron Transfer

As stated in I, projectiles may also effect target K-shell ionization by capturing target K-shell electrons into vacant bound states. Presented in this section are theoretical formulations of target K-shell to projectile K,L,M,N ...-shell electron transfer cross section calculations.

Oppenheimer[11] and Brinkman and Kramers[12] in 1928 and 1930, respectively, developed the basis for what is today known as the Oppenheimer Brinkman Kramers (OBK) approximation. The theory was originally limited

FIGURE 2

(a) Direct Coulomb ionization cross sections for ^{16}O ions on Al showing the relative magnitudes of PWBA, PSS(CBP), and PSS(CB) calculations.

(b) Direct Coulomb ionization cross sections for ^{16}O ions on Al showing the relative magnitudes of PWBA, NPSS(CB), and NPSS(CBP) calculations.

$^{16}O \rightarrow Al(K)$

(a)

PWBA
PSS(CBP)
PSS(CB)

(b)

PWBA
NPSS(CBP)
NPSS(CB)

σ_K^i (b)

E_1 (MeV)

12
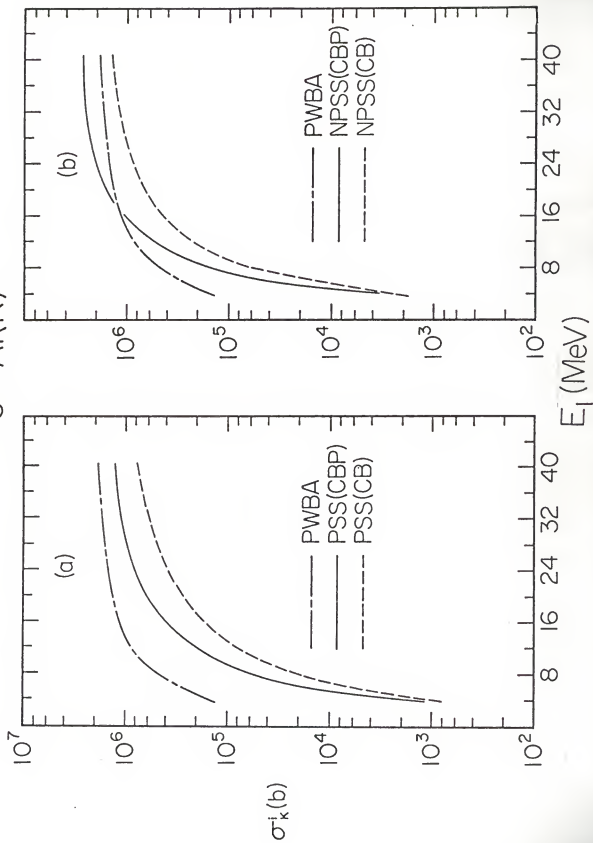
to calculation of electron capture by bare projectiles from hydrogen-like targets, but in 1967 Nikolaev[13] extended the theory to include capture from any closed shell atom.

Theoretical target K-shell to projectile K-shell (K-to-K) electron transfer cross sections ($\sigma_{2K \to K}$) may also be calculated from the theory of Lapicki and Losonsky (LL)[14] which is based on the OBK approximation with binding and Coulomb deflection corrections at low scale velocities. Lapicki and Losonsky[14] state however that $\sigma_{K \to L, M, N \ldots}$ cannot be accurately calculated by this method. The "2" in $\sigma_{2K \to K}$ serves as a reminder that there are two projectile K-shell vacancies. If one disregards the fact that projectiles with one vs two K-shell vacancies have different K-shell binding energies, then a simple statistical model would require the electron transfer cross section for the case of one projectile K-shell vacancy, $\sigma_{1K \to K}$, to be $\sigma_{2K \to K}/2$.

In this notation, electron transfer cross sections from target K-shell to projectile K-shell are noted by $\sigma_{2K \to K}(>>)$ and $\sigma_{2K \to K}(<<)$, where ($<<$) and ($>>$) refer to the velocity regions $v_1 \gg v_{2K}$, v_{1K} and $v_1 \ll v_{2K}$, v_{1K}, respectively. Here, v_{1K} is the projectile K-shell average orbital velocity, v_{2K} the target K-shell average orbital velocity. The ($>>$) region is arbitrarily extended by LL to cover the region $v_1 \gtrsim v_{2K}$, v_{1K}, and is noted as $\sigma_{2K \to K}(\gtrsim)$. In the region where $v_1/v_{2K} \simeq 1$, the cross section for K-to-K electron transfer is found by the use of interpolation as given by LL,[14] i.e.

$$\sigma_{2K \to K(LL)} = \frac{(\sigma_{2K \to K}(\gtrsim) \; \sigma_{2K \to K}(<<))}{\sigma_{2K \to K}(\gtrsim) + (2/3) \; \sigma_{2K \to K}(<<)} \; . \quad \text{eq.II.B.1}$$

13

Explicitly, the LL cross sections are given by

$$\sigma_{2K \to K}(\geq) = (1/3)\ \sigma_{2K \to K(OBK)}(\theta_K)$$

and

$$\sigma_{2K \to K}(<<) = \exp\left(-\pi d_{KK}\ q_{KK}\ (\epsilon_K \theta_K)\right)\sigma_{2K \to K(OBK)}(\epsilon_K \theta_K)$$

with

$$\sigma_{2K \to K(OBK)}(\theta_K) = \pi a_o^{\ 2}(2^9/5v_1^{\ 2})\frac{(v_{1K}v_{2K})^5}{(v_{1K}^{\ 2}+(v_1^{\ 2}+v_{2K}^{\ 2}-v_{1K}^{\ 2})^2/4v_1^{\ 2})^5} \quad \text{eq.II.B.2}$$

In this calculation θ_K at low scale velocities is replaced by $\epsilon_K \theta_K$ and hence the cross section is $\sigma_{2K \to K(OBK)}(\epsilon_K \theta_K)$.

The relevant quantities required for the LL calculation are:

$$\theta_K = \hbar\omega_{2K}/Z_{2K}^{\ 2}\ 13.6\ eV,$$

$$a_o = \hbar^2/m_e e^2 = 5.39 \times 10^{-9}\ cm \quad,$$

$$v_{1K} = Z_1 \quad,$$

$$v_{2K} = Z_{2K} = Z_2 - 0.3 \quad,$$

$$d_{KK} = d(1 - (v_{2K}^{\ 2}\theta_K - v_{1K}^{\ 2})/v_1^{\ 2}M)^{-1/2} \quad,$$

$$\text{with } d = Z_1 Z_2/v_1^{\ 2}M \quad,$$

$$1/M = 1/M_1 + 1/M_2 \quad,$$

$$q_{KK}(\theta_K) = (v_{2K}^{\ 2}\theta_K - v_{1K}^{\ 2})/2v_1 + v_1/2 \quad,$$

$$\epsilon_K = 1 + (2Z_1/Z_{2K}\theta_K)g_K(v_{2K}/\beta^{1/2}) \quad,$$

$$\beta = q_{KK}^{\ 2} + v_{1K}^{\ 2} \quad,$$

14

$$g_K(z) = (1 + 5z + 7.14z^2 + 4.27z^3 + 0.95z^4)/(1 + z)^5 \quad .$$

When $\theta_K \to \epsilon_K \theta_K$, $v_{2K} \to \epsilon_K^{1/2} v_{2K}$. The $\exp(-\pi d_{KK} q_{KK}(\epsilon_K \theta_K))$ factor is a Coulomb deflection correction, which is applicable only at low scale velocities, and $\theta_K \to \epsilon_K \theta_K$ accounts for increased target K-shell binding, also a low velocity effect.

Theoretical target K-shell to projectile L,M,N...-shell electron transfer cross sections ($\sigma_{K \to L,M,N \ldots}$) are calculated in the OBK approximation of Nikolaev[13], $\sigma_{K \to L,M,N \ldots (OBK)}$, and scaled by semiempirical scale factors (sf) taken from Guffey.[15] It was shown by Guffey that for N and F ions on Kr and Ar thin gas targets the total single-capture OBK cross sections were factors of ~5-50 times larger than the experimentally measured single capture cross sections, depending on projectile energy. For this work, the sf for N and F ions on Al were extrapolated from the Kr and Ar data and hence provide semi-empirical corrections for the $\sigma_{K \to L,M,N \ldots (OBK)}$ electron transfer cross section calculations. The N and F sf values were averaged to give scale factors for O ions on Al, because no O on Kr and Ar sf data was available. Thus,

$$\sigma_{K \to L,M,N \ldots} = \sigma_{K \to L,M,N \ldots (OBK)} \Big/ sf \quad .$$

Where there is no screening, the expression for $\sigma_{K \to L,M,N \ldots (OBK)}$ is

$$\sigma_{K \to L,M,N \ldots} = \pi a_o^2 n_1^2 (2^9/5)(V_o/V)^2 \gamma^5 \eta_n^2 \quad \text{eq.II.B.3}$$

where

$$a_o = \hbar^2/e^2 m_e = 5.29 \times 10^{-9} \text{cm}$$

$$v_o = e^2/\hbar \quad ,$$

$n_1 = 2,3,4\ldots$ (principal quantum number of the final state of the electron in the projectile),

15

$$\eta_n = v_{1L,M,N\ldots}/v_{2K} = (Z_1^2 \ 13.6 \ eV/n_1^2 \hbar\omega_{2K})^{1/2} \ ,$$

$$V = v_1/v_{2K} \ ,$$

$$\gamma = 4(1 + 2(1+\eta_n)V^{-2} + (1 - \eta_n^2)^2 V^{-4})^{-1} V^{-2} \ .$$

C. Target Thickness Effects

It has been well established[16-21] that measured target K x-ray production cross sections are strongly dependent on target thickness ρx for $Z_1/Z_2 \gtrsim 0.3$. When heavy ions with i K-shell vacancies, $i=0,1,2$, are incident on a solid target, interactions with the target material will in general cause projectile K-shell vacancy production and quenching. At any given depth z within the target the beam will consist of three fractions, $Y_i(z)(i = 0,1,2)$, that represent portions of the beam with i K-shell vacancies. At all depths, $\sum_0^2 Y_i(z) = 1$. The $Y_i(z)$ have in general complicated exponential dependences[17] on depth and the projectile K-shell vacancy production and quenching cross sections, $\sigma_{ij}(i = 0,1,2, \ j = 0, 1,2, \ i \neq j)$ as defined in Ref. 17.

A different target ionization cross section must be associated with each projectile K-vacancy fraction because of the possibilities for K-to-K electron transfer contributions to the target K-shell ionization cross section for projectiles with i K-shell vacancies, as first pointed out by Halpern and Law.[22] Written in terms of target K x-ray production cross sections, the various contributions to the production of target K x rays for projectiles with i K-shell vacancies are defined as $\sigma_{Ki}(i = 0,1,2)$. For any given thickness target $\rho x=T$ (where T is sufficiently small so that energy loss and projectile K-shell vacancy fraction equilibration[17] are not overriding factors) the measured target K

16

x-ray production cross section will be the average of the three indivi-
dual cross sections weighted by their respective fractions,[17]

$$\overline{\sigma}_{Kx}(T) = (1/T) \int_0^{T_2} \sum_0 \sigma_{Ki} Y_i(z) dz \quad .$$

The $Y_i(z)$ are subject to initial conditions so that $Y_i(z = 0) \{ {}^{=1}_{=0} \}$ for
$i\{ {}^{=}_{\neq} \}$ to the number of K-shell vacancies in the incident beam. If the
target is very thin, $T \simeq 0$, the initial K-shell vacancy fraction is
nearly equal to one, and in the limit $T \rightarrow 0$, the x-ray production cross
section becomes

$$\overline{\sigma}_{Kx}(T) = (1/T) \int_0^T \sigma_{Ki} dz = \sigma_{Ki} \quad .$$

$$\text{Limit } T \rightarrow 0$$

For practical reasons, experimental determination of σ_{Ki} then requires
that measurements be made with a series of different thickness targets,
where the σ_{Ki} are determined by extrapolation of $\overline{\sigma}_{Ki}(T)$ to $T = 0$.

By consideration of semi-empirical post-foil charge state frac-
tions of 0 ions,[23] it can be seen that there are a consider-
able number of projectile L-shell vacancies present over a broad range
of energies. See e.g. Fig. 3 from Ref. 23. Therefore, target K-shell
electron transfer into the projectile L-shell should depend only weakly
on the projectile L-shell configuration prior to its striking the target.
It follows then that any theoretical model for target K-shell ionization
should necessarily include consideration of target K-shell to projectile
L- and also M,N...-shell electron transfer contributions, independent
of the number of projectile K-shell vacancies. Note: Target K-shell
electron capture to the projectile continuum[14] and excitation to higher

FIGURE 3

Semi-empirical post-foil charge state fractions of O ions as a function of energy from Ref. 23.

OXYGEN

ϕ_8

ϕ_7

ϕ_6

ϕ_5

ϕ_4

MeV/A
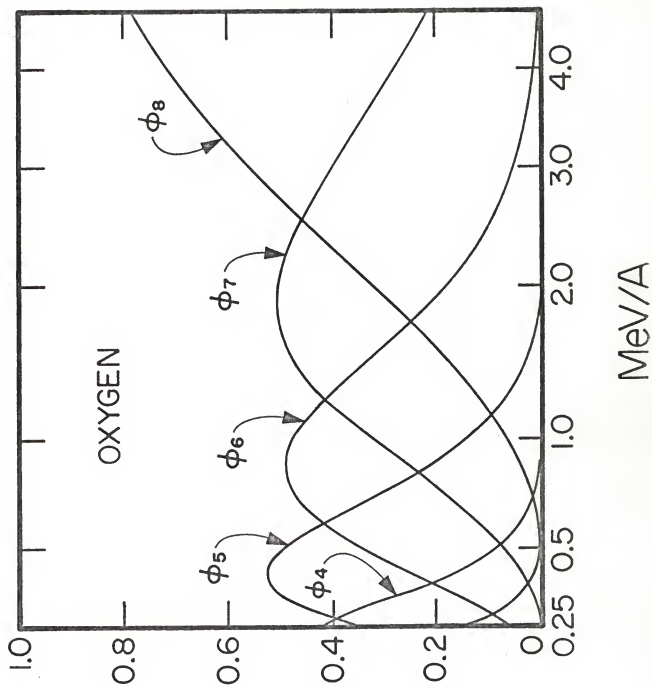
bound target states[5] are taken to be insignificant contributions to the total target K-shell ionization cross section.

D. Fluorescence Yields

Appropriate fluorescence yields are necessary to compare the theoretical ionization cross sections to the experimental x-ray production cross sections. Previous Si K x-ray satellite spectra[24] for incident ^{19}F ions has shown that the K-shell fluorescence yield $\bar{\omega}_K = 1.5\ \omega_K$, where ω_K is the neutral atomic fluorescence yield. Other results[25] for ^{16}O ions on Al are very similar. Thus through the use of configuration fluorescence yields[26] and the results for both Si and Al targets, it is taken that $\bar{\omega}_K = 1.5\ \omega_K = 0.057$, independent of projectile energy, ion species, and number of K-shell vacancies.

E. Summary of Theory

Direct Coulomb ionization and electron transfer processes are independent because they have different final states. Thus the target K x-ray production cross sections in the limit T = 0 are additive, and the following expressions result:

$$\sigma_{K0} = \sigma_{K(DC)}^x + \sigma_{K \to L,M,N...}^x$$

and

$$\sigma_{Ki} = \sigma_{K0} + \sigma_{iK \to K}^x \quad (i = 1,2) \quad,$$

where

$$\sigma_{K(DC)}^x \equiv \bar{\omega}_K \sigma_{K(DC)} \quad,$$

$$\sigma_{iK\ K}^x \equiv \bar{\omega}_K \sigma_{iK \to K} \quad,$$

and

$$\sigma_{K \to L,M,N...}^x \equiv \bar{\omega}_K \sigma_{K \to L,M,N...} \quad.$$

The K-to-K electron transfer cross sections are then given as

$$\sigma_{iK \to K}^{x} = \sigma_{Ki} - \sigma_{K0} \quad (i = 1,2) \quad .$$

In the notation of Ref. 17,

$$\sigma_{K1} = \alpha\sigma_{K0} \quad \text{and} \quad \sigma_{K2} = \beta\sigma_{K0}$$

where

$$\alpha = (\sigma_{K0} + \sigma_{1K \to K}^{x})/\sigma_{K0} \quad \text{and} \quad \beta = (\sigma_{K0} + \sigma_{2K \to K}^{x})/\sigma_{K0} \quad .$$

Sample calculations of the theoretical direct Coulomb ionization and electron transfer cross sections given in II A. and II B. for 1.0 MeV/amu N ions on Al are presented in the Appendix. The PSS and NPSS direct Coulomb ionization, Lapicki and Losonsky K-to-K electron transfer, and OBK K-to-L,M,N... electron transfer cross sections for 0.6–2.2 MeV/amu N, O, and F ions on Al are given in Tables I–III, respectively. The N, O, and F on Al sf values, and scaled OBK K-to-L,M,N... electron transfer cross sections are also included in Table III.

TABLE I

Theoretical Al K-Shell Direct Coulomb Ionization Cross Sections[a]

$$\sigma_{K(DC)} (10^5 b)$$

E_1/M_1 (MeV/amu)	N→Al(K)			O→Al(K)			F→Al(K)		
	NPSS(CBP)	NPSS(CB)	PSS(CB)	NPSS(CBP)	NPSS(CB)	PSS(CB)	NPSS(CBP)	NPSS(CB)	PSS(CB)
0.6	2.39	1.04	0.36	2.84	1.11	0.33	3.28	1.15	0.30
0.8	5.42	2.32	0.86	6.90	2.63	0.86	8.50	2.88	0.82
1.0	8.62	3.78	1.53	11.3	4.43	1.59	14.4	5.03	1.60
1.2	11.5	5.19	2.27	15.4	6.23	2.44	20.0	7.26	2.55
1.4	13.9	6.47	3.01	18.9	7.87	3.33	24.8	9.32	3.56
1.6	15.7	7.58	3.73	21.5	9.34	4.20	28.4	11.2	4.57
1.8	17.2	8.54	4.38	23.5	10.6	5.02	31.2	12.8	5.54
2.0	18.2	9.35	4.97	24.9	11.7	5.76	33.2	14.1	6.44
2.2	18.9	10.0	5.49	25.9	12.6	6.41	34.6	15.3	7.26

(a) Calculations are based upon Refs. 7 and 9.

TABLE II

Theoretical Cross Sections[a] for Al K-Shell to Projectile K-Shell Electron Transfer

$$\sigma_{1K \to K(LL)} \quad (10^5 b)$$

E_1/M_1 (MeV/amu)	N→Al(K)		O→Al(K)		F→Al(K)	
	$i=1$	$i=2$	$i=1$	$i=2$	$i=1$	$i=2$
0.6	0.92	1.84	2.06	4.12	4.42	8.84
0.8	1.76	3.52	3.67	7.33	7.20	14.4
1.0	2.59	5.17	5.0	10.2	9.45	18.9
1.2	3.27	6.54	6.20	12.4	11.0	21.9
1.4	3.76	7.52	7.00	13.9	11.9	23.7
1.6	4.06	8.13	7.30	14.6	12.2	24.3
1.8	4.21	8.42	7.45	14.9	12.1	24.2
2.0	4.23	8.45	7.35	14.7	11.7	23.4
2.2	4.15	8.30	7.15	14.3	11.2	22.4

[a]Calculations are based upon Ref. 14.

TABLE III

Theoretical Cross Sections[a] for Al K-Shell to Projectile

L,M,N ...-Shell Electron Transfer

E_1/M_1 (MeV/amu)	N→Al(K)			O→Al(K)			F→Al(K)		
	$\sigma_{K \to L,M,N \ldots}$(OBK) ($10^5$ b)	sf[b]	$\sigma_{K \to L,M,N \ldots}$ (10^5 b)	$\sigma_{K \to L,M,N \ldots}$(OBK) ($10^5$ b)	sf[b]	$\sigma_{K \to L,M,N \ldots}$ (10^5 b)	$\sigma_{K \to L,M,N \ldots}$(OBK) ($10^5$ b)	sf[b]	$\sigma_{K \to L,M,N \ldots}$ (10^5 b)
0.6	0.27	34	13.6	0.66	30.8	20.2	1.48	28.5	42.0
0.8	0.56	24.5	13.6	1.23	23.5	29.2	2.48	23.5	58.2
1.0	0.97	17.5	16.9	1.87	18.8	35.2	3.44	20.0	68.6
1.2	1.40	13.5	18.9	2.62	14.8	38.8	4.47	16.5	73.9
1.4	1.72	11.5	19.8	3.14	12.8	40.1	5.81	13.0	75.6
1.6	1.99	10.0	19.9	3.82	10.5	40.0	7.03	11.0	77.3
1.8	1.96	10.0	19.6	4.10	9.5	38.9	7.15	10.0	71.5
2.0	1.90	9.9	18.8	4.35	8.5	37.1	9.0	7.5	67.8
2.2	1.80	9.9	17.8	4.35	8.0	34.9	1.06	6.0	63.4

(a) Calculations are based upon Ref. 13.

(b) The scale factors are derived from Ref. 15.

III. EXPERIMENTAL PROCEDURE

A. Experimental Cross Section Calculation Method

When projectiles are incident on a thin solid target of thickness T, the yield Y_p of elastically scattered projectiles and the target K x-ray yield $Y_{xi}(T)$ are written as

$$Y_p = N\phi\sigma(\theta)_R \Delta\Omega_p \epsilon_p \qquad \text{eq. III.A.1.}$$

$$Y_{xi}(T) = N\phi\overline{\sigma}_{Kx}(T)\Delta\Omega_x \epsilon_x \qquad \text{eq. III.A.2.}$$

where: N = number of target atoms per unit area,

ϕ = number of projectiles to strike target,

$\sigma(\theta)_R$ = Rutherford nuclear elastic scattering cross section for projectiles scattering from target nucleii at lab angle θ,

$\overline{\sigma}_{Kx}(T)$ = average target K x-ray production cross section for a given thickness target T and initial projectile K-shell vacancy number,

$\Delta\Omega_p$ = effective solid angle subtended by particle detector,

$\Delta\Omega_x$ = effective solid angle subtended by x-ray detector,

ϵ_p = efficiency of particle detector,

ϵ_x = efficiency of x-ray detector for specific energy.

Here (T) serves as a reminder that the quantities are functions of target thickness. By dividing eq. III.A.1. by eq. III.A.2. and rearranging,

$$\overline{\sigma}_{Kx}(T) = (Y_{xi}(T)/Y_p)\sigma(\theta)_R(\Delta\Omega_p/\Delta\Omega_x)(\epsilon_p/\epsilon_x) \qquad \text{eq. III.A.3.}$$

Assuming that ϵ_p remains constant with energy over a sufficient range, then

$$\overline{\sigma}_{Kx}(T) = (Y_{xi}(T)/Y_p)\sigma(\theta)_R K \qquad \text{eq. III.A.4.}$$

where K is a constant. The Rutherford nuclear elastic scattering cross section is given by[27]

$$\sigma(\theta)_R = 1.296 \; (Z_1 Z_2/E_1)^2 (\csc^4(\theta/2) - 2(M_1/M_2)^2 \cdots) \text{mb/sr}$$

where the next term is order $(M_1/M_2)^4$, and where:

Z_1 = projectile atomic number,

Z_2 = target atomic number,

E_1 = projectile energy (MeV),

θ = scattering angle in the lab,

M_1 = projectile mass (amu),

M_2 = target mass (amu).

If $\theta = 30^{\circ}$, then $\csc^4(\theta/2) = 222.85$, and for N, O, and F ions on Al, $2(M_1/M_2)^2 = 0.5$, 0.7, and 1.0, respectively. An approximation that is accurate to error less than 0.5% is then

$$\sigma(\theta)_R = 1.296 \; (Z_1 Z_2/E_1)^2 \csc^4(\theta/2) \text{mb/sr} \qquad \text{eq. III.A.5.}$$

Hence

$$\overline{\sigma}_{Kx}(T) = (Y_{xi}(T)/Y_p)(Z_1/E_1)^2 K' \qquad \text{eq. III.A.6.}$$

where $K' = K Z_2^2 \; 1.296 \; \csc^4(\theta/2) \text{mb/sr}$. However the σ_{Ki}, rather than $\overline{\sigma}_{Kx}(T)$, are the cross sections of interest. Rather than calculating all of the $\overline{\sigma}_{Kx}(T)$ by this method and then extrapolating to $T = 0$, the $Y_{xi}(T)/Y_p$ may be extrapolated to $T = 0$. This gives the Y_{xi}/Y_p values, which can be used to evaluate

$$\sigma'_{Ki} = \sigma_{Ki}(Y_{xi}/Y_p)' \; (Z_1/E_1)'^2 \; / \; (Y_{xi}/Y_p)(Z_1/E_1)^2 \quad \text{eq. III.A.7.}$$

where one σ_{Ki} and corresponding Y_{xi}/Y_p are known.

B. Experimental Apparatus

Aluminum targets were prepared by evaporating solid Al onto 20 $\mu g/cm^2$ self supporting carbon foils. The carbon foils, from Arizona Carbon Foil Company, were floated from glass backings in water and then lifted onto polished stainless steel target frames. The carbon was allowed to dry, and the Al was deposited by evaporation in a ~ 1×10^{-7} Torr vacuum. Approximately 40 targets were made, varying in thickness from T ≃ 1 - 50 $\mu g/cm^2$. Aluminum thicknesses were measured by Rutherford scattering of 600 KeV protons, from a 3 MV AK-N Van de Graaff accelerator, at $150°$ in the lab. Data for the target K x-ray production by N^{+q}, O^{+q}, and F^{+q} beams was taken with the 6 MV EN Tandem Van de Graaff accelerator facility at Kansas State University. At a given terminal voltage, the Tandem Van de Graaff produces different species of high energy ions at several different charge states and corresponding energies. At $90°$ analyzing magnet is used to select a particular species of ion with specific charge state and energy. Both 5 and 10 $\mu g/cm^2$ carbon post-stripping foils are available downstream of the analyzing magnet for further stripping of the projectile as required. A beam line switching magnet is used to select the proper charge state of post-stripped ions. In this manner well defined monoenergetic ions of the desired charge states are available for the experiment.

To preclude the possibility of any unknown $1s2s^3S_1$ He-like metastable fraction of the beam, only the Z_1, Z_1-1, and < Z_1-2 charge states should be used in experiments of this type. The reason for this is that the unknown metastable fraction of the Z_1-2 beam is sufficiently long lived,[28] considering path length and velocity, to deliver some projectiles to the target with one K-shell vacancy rather than zero. Therefore any

σ_{KO} measured using Z_1-2 charge state projectiles will be increased by approximately 10%.

A schematic of the facility is shown in Fig. 4, from which N, O, and F ions of incident charge states Z, Z-1, and < Z-2 in the energy range of 0.6 - 2.2 MeV/amu were available. Because of energy considerations N^{+5} ions were used to achieve incident N energies of 2.0 and 2.2 MeV/amu.

The target area is shown schematically in Fig. 5. Five targets at one time were mounted on a vertical rod, which serves to locate the targets on the beam axis. The rod is capable of rotation about the vertical axis, as well as linear vertical motion. Targets could be changed and rotated for differing thicknesses without opening the vacuum system. A vacuum of approximately 1×10^{-6} Torr was maintained in the region of the target. Targets were rotated at an angle $\phi = 20^\circ$ toward the x-ray detector, from perpendicular to the beam axis. With the 20° rotation, the zero angle thicknesses were effectively increased to

$$T(20^\circ) = T(0^\circ)/\cos 20^\circ = 1.06 \ T(0^\circ).$$

Two 3 mm diameter collimators, separated by 150 mm, defined the beam geometry. The last collimator was located approximately 2.5 cm away from the target. Care was taken that none of the beam could scatter around the outside of the collimators, and adjustable slits were used to decrease the beam current just upstream of the collimators, if necessary. An Ortec Si(Li) x-ray detector was placed inside the vacuum system, 125 mm from the target beam spot and 90° from the beam axis. Count rates were restricted to ≤ 1000 cps to minimize dead time corrections. Scattered particles were detected at 30° from the beam axis, so that the $\sigma(\theta)_R$ approximation of eq. III.A.6. would be valid. Statistical errors in the Al K x-ray and scattered particle yields were $\leq 2\%$ and 5%, respectively.

FIGURE 4

Schematic of the Tandem Van de Graff facility at Kansas State University used for the production of N, O, and F heavy ions.

SCHEMATIC DIAGRAM OF THE ACCELERATOR FACILITY USED FOR THE PRODUCTION OF HEAVY PROJECTILE IONS

A DIODE ION SOURCE
B INFLECTION MAGNET
C TANDEM VAN DE GRAAFF
D QUADRUPOLE LENSES
E ANALYZING MAGNET
F POST STRIPPING FOIL
G SWITCHING MAGNET
H TARGET AREA
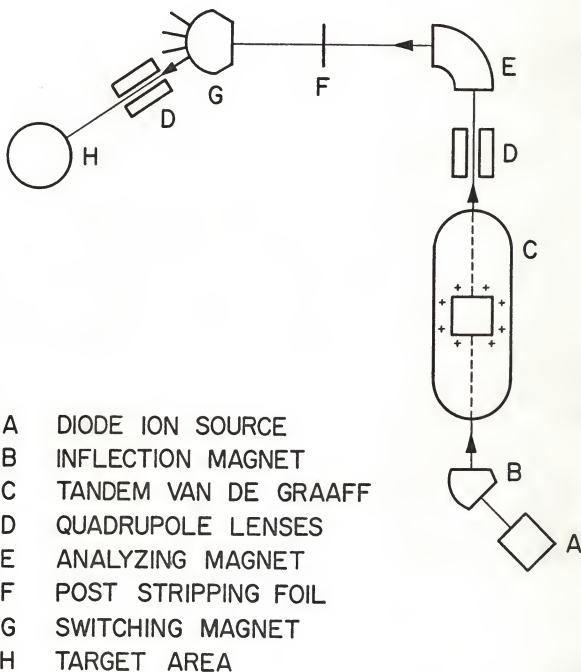
FIGURE 5

Schematic of the experimental arrangement used in the measurement of Al K x-ray production cross sections for N, O, and F heavy ion bombardment.

SCHEMATIC OF TARGET AREA USED
FOR MEASUREMENT OF Al(K) X-RAY
PRODUCTION CROSS SECTIONS
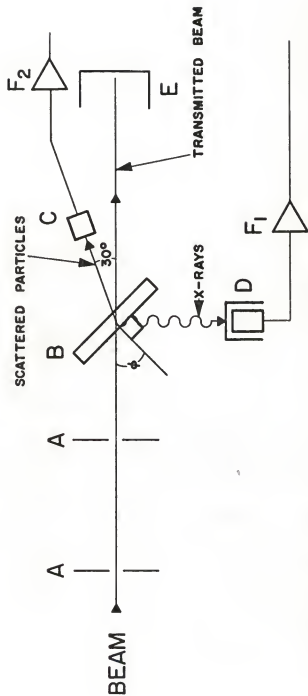
A   COLLIMATORS
B   THIN Al TARGET
C   SURFACE BARRIER PARTICLE DETECTOR
D   Si(Li) X-RAY DETECTOR
E   FARADAY CUP
F_1 Si(Li) DETECTOR PRE-AMP
F_2 PARTICLE DETECTOR PRE-AMP

BEAM

SCATTERED PARTICLES

30°

TRANSMITTED BEAM

X-RAYS

32

A schematic diagram of the electronics used is given in Fig. 6, and a list of components given in Table IV.

A Faraday cup with -300 volt secondary electron suppression ring was used for integration of the beam when necessary. Data was taken in 0.2 MeV/amu increments.

C. Corrections to Data

Corrections made to the experimental data are noted in this section.

1. Projectile Radiative Electron Capture (REC)

If the projectile captures an Al or C outer-shell electron into a K-shell vacancy, an x-ray of higher than characteristic projectile K x-ray energy may result. This is termed radiative electron capture (REC),[29] and is due to the increased kinetic energy of the electron with respect to the projectile due to their relative velocities. In the case of all N, O, and F projectiles, part of the REC distribution fell under the Al K x-ray energy peak, Al(K), at all projectile energies. An example of such an REC distribution is shown in Fig. 7, where no Al was present on the carbon foil. The Al(K) energy window is noted for comparison. To determine REC contributions, the REC count per unit integrated beam current was measured for the bare carbon foil at all energies. By also integrating the beam current while taking target K x-ray production data, it was straightforward to subtract an amount of REC proportional to the integrated beam from the Al(K) energy window using the relationship

$$Y_{xi}(T) = Y'_{xi}(T) \left[1 - Q(Al + C)(Y_{REC}/Q(C)) \right] \quad \text{eq. III.C.1}$$

where:

$Y_{xi}(T)$ = corrected Al K x-ray yield ,

$Y'_{xi}(T)$ = uncorrected Al K x-ray yield ,

33

FIGURE 6

Schematic diagram of electronics used in experiment.

X-RAY DETECTOR A — PRE-AMP C — AMP D — DIG. TO ANALOG F — PDP 15 G

BIAS B

SCOPE

COUNT RATE METER E

FARADAY CUP — CURRENT INTEGRATE H — SCALER I

PARTICLE DETECTOR J — PRE-AMP K — AMP M — MCA N

BIAS L

SCOPE

35
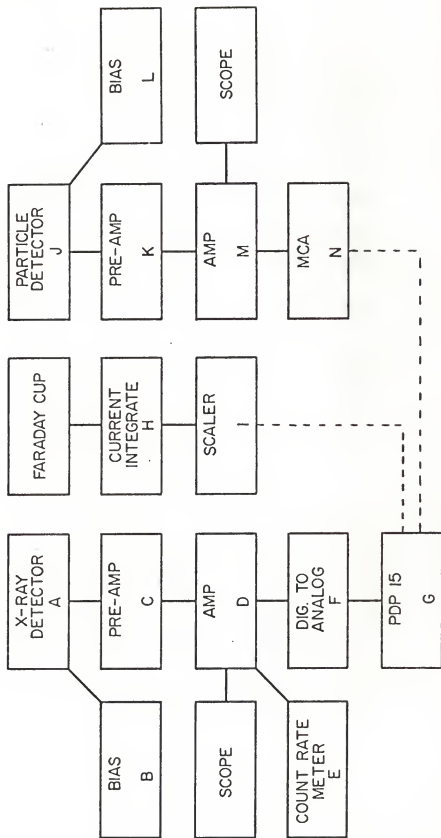
TABLE IV

List of Electronics Components Shown in Fig. 6

A ORTEC MOD 7113-04160-5 Si(Li) DECTECTOR (-1500V Bias)

B ORTEC MOD 456 HIGH VOLTAGE POWER SUPPLY

C ORTEC MOD 117B PRE-AMP

D ORTEC MOD 450 RESEARCH AMP

E ORTEC MOD 441 RATEMETER

F geos MOD 8050 ANALOG TO DIGITAL CONVERTER

G Digital Equipment Corporation PDP-15 COMPUTER

H BIC MOD 1000 CURRENT INTEGRATOR

I CANBERRA MOD 1776 DUAL COUNTER/TIMER

J ORTEC 17-477A SURFACE BARRIER DETECTOR (+100V Bias)

K CANBERRA MOD 1408 PRE-AMP

L ORTEC MOD 216 HIGH VOLTAGE POWER SUPPLY

M TENNELEC MOD TC 203BLR LIN AMP

N CANBERRA MOD 8100 MULTICHANNEL ANALYZER

FIGURE 7

Radiative electron capture (REC) distribution for O ions on a 20 ug/cm^2 carbon target. The O K x-ray peak and Al K x-ray energy window are also noted.

X-RAY PRODUCTION
1.4 MeV/amu O^{+4} ⟶ C (20 μg/cm^2)

O(K)

O(REC)

Al(K) ENERGY WINDOW

COUNTS PER CHANNEL

CHANNEL NUMBER
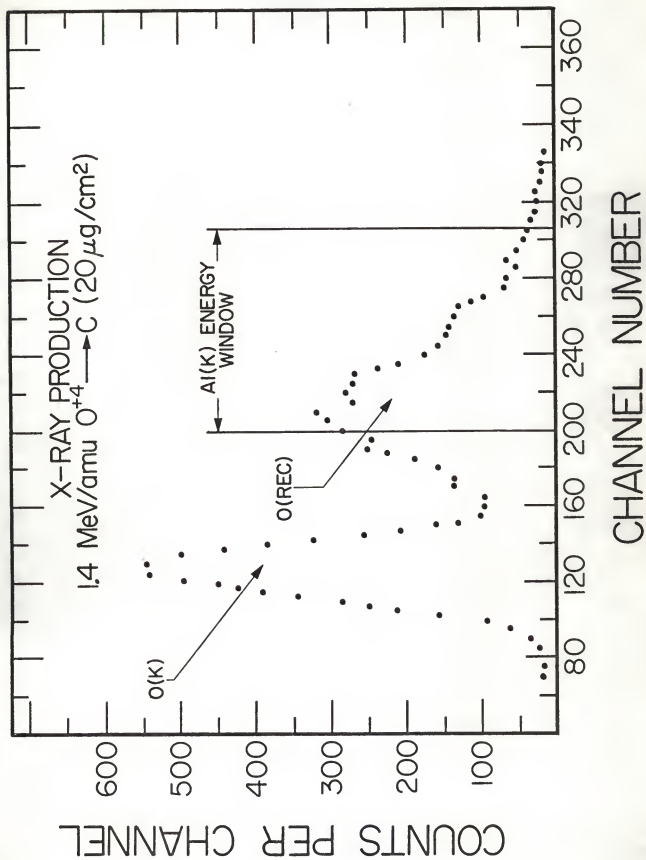
$Q(Al + C)$ = integrated beam current during collection of $Y'_{x1}(T)$,

$Y_{REC}/Q(C)$ = number of REC's in Al(K) energy window per unit

integrated beam current with only carbon foil present.

Typical corrections were ~ 2 - 20%. If the corrections were accurate
to ~±25%, then the $Y_{x1}(T)$ should have been correct to ~±1 - 5%, dis-
counting statistical errors.

2. $1s2s^3s_1$ Metastable Fraction

Because only N^{+5} and not N^{+4} was available at 2.0 and 2.2 MeV/amu
the σ^x_{KO}, $\sigma^x_{1K \to K}$, and $\sigma^x_{2K \to K}$ values in these cases were changed by an amount
consistent with the ~10% effect due to the $1s2s^3S_1$ fraction as observed
in the case of O^{+6} ions on Al in Fig. 8.

3. Non-Rutherford Scattering

At higher energies (~1.8 - 2.2 MeV/amu) the nuclear elastic scatter-
ing from the Al became non-Rutherford.[30] Because of this, eq. III.A.6.
was not valid. To correct this, approximately 10 ug/cm^2 of Au was eva-
porated over a 26.5 ug/cm^2 Al target. The N, O, and F ion beams were
run on this target at energies from ~1.4 - 2.2 MeV/amu, where scattering
from Au is Rutherford throughout.[30] By measuring $Y_{p(Al)}/Y_p(Au)$, the
$Y_{p(Al)}$ values at specific energies can be corrected to account for non-
Rutherford scattering according to

$$Y_p = Y_p'/C$$

where: Y_p = corrected particle yield at a given energy,

Y_p' = uncorrected particle yield at a given energy.

The N, O, and F nuclear elastic scattering from Al is Rutherford at 1.4
MeV/amu, so the $Y_{p(Al)}/Y_{p(Au)}$ values were normalized to this point.
Hence the values of C are given by

FIGURE 8

Ratio of Al K x-ray yield per elastically scattered O^{+q} ions for q = 4-8 for 1.4 ug/cm^2 Al target.

NON—RUTHERFORD PROJECTILE
SCATTERING CORRECTION
FACTOR

N, O, F, ——→Al, Au
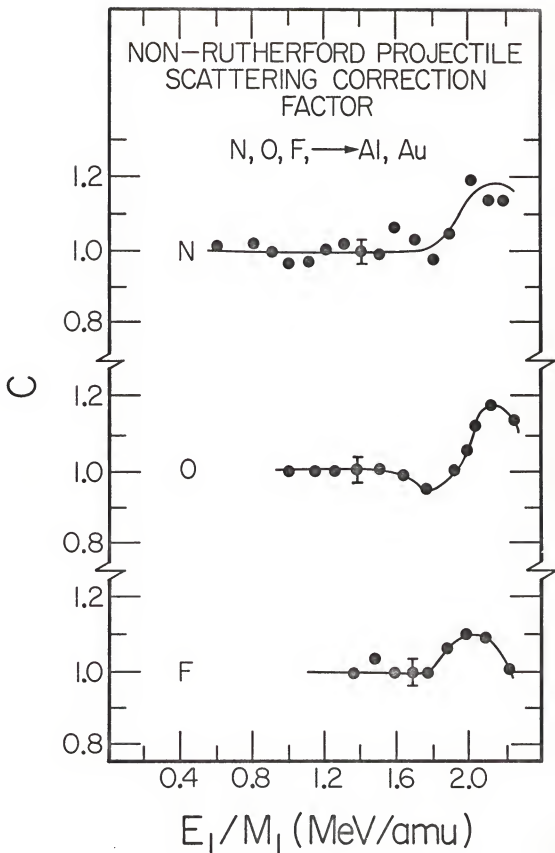
$$C = \frac{(Y_{p(Al)}/Y_{p(Au)})(E_1/M_1)}{(Y_{p(Al)}/Y_{p(Au)})(1.4 \text{ MeV/amu})} \quad , \qquad \text{eq. III.C.2}$$

and are shown in Fig. 9.

It was determined that changes in $\sigma(\theta)_R$ due to projectile energy losses within the target material[31] were < 0.2%.

FIGURE 9

Correction factors for non-Rutherford nuclear elastic scattering of N, O, and F ions from Al. The lines are to guide the eye.

NON−RUTHERFORD PROJECTILE
SCATTERING CORRECTION
FACTOR

N, O, F, —→Al, Au

E_1 / M_1 (MeV/amu)
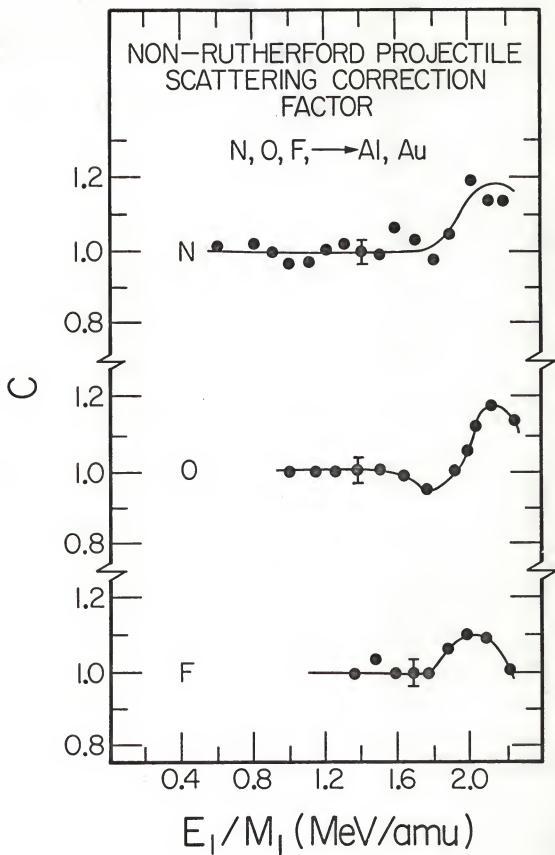
IV. RESULTS AND ANALYSIS

A. Projectile K-Shell Vacancy Effects in Inner-Shell Ionization

The role of projectile K-shell vacancies in heavy ion-induced target K x-ray production for $Z_1/Z_2 \sim 0.6$ is clearly exemplified in Fig. 8 which demonstrates the strength of the target K-shell to projectile K-shell (K-to-K) electron transfer process. Increases in the ratio of target K x rays per scattered particle, Y_x/Y_p for incident ions with initial charge states $q \leq Z_1 - 3$ is essentially constant, thus indicating that target K-shell ionization is not dependent upon the number of L-shell electrons on the incident ion.

Furthermore the lack of dependence of Y_x/Y_p on the number of L-shell electrons on the projectile indicates that for heavy ions on solid targets the fluorescence yield does not change with the incident charge state as observed in gasses.[32] This feature of heavy ion bombardment of solid targets has recently been directly observed by Richard et al.[32] in studies of high resolution x-ray spectroscopy for F ions on thin solid Si and gaseous SiH_4 targets. They observe that the x-ray satellite energy spectra for the solid are independent of the incident charge state, thus indicating that the F ions travel through the solid with an average charge state which is determined for distances into the solid which are small in comparison to the thickness of the thin solid.

The $\sim 10\%$ increase in the target K x-ray yield for O^{+6} ions is attributed to the $1s2s\,^3S_1$ metastable fraction of the beam. Charge state dependence such as that exhibited in Fig. 8 is a necessary condition for the observation of target thickness dependences of target K x-ray production for heavy ions incident upon solids. If this condition is fulfilled and there are stong projectile K-shell vacancy production

45

processes affecting the ion in the solid, then target K x-ray production
will exhibit target thickness dependences.

B. Target Thickness Effects

The effect of target thickness in determining target K x-ray pro-
duction for heavy ions incident with i K-shell vacancies (i=0,1,2) is
given in Fig. 10 for 1.0 MeV/amu O^{+q}(q=4,7,8) ions on thin Al targets.
Similar behavior was observed for N, O, and F projectiles at all energies.
Cross sections for Al K x-ray production were obtained by normalization
to the data of Tawara et al.[35] for H ions on Al. This normalization pro-
cedure gives

$$\sigma_{KO}(1.0 \text{ MeV/amu } O^{+4} \rightarrow Al(K)) = 2.0 \times 10^4 b \pm 20\%.$$

Also demonstrated in Fig. 10 is the need for a clear understanding of the
target thickness effects and the presence of K-to-K electron transfer
when target K x-ray production cross sections for heavy ions are measured.
As set forth in II C., measurements of target K x-ray production cross
sections at non-zero target thickness give only a weighted average of
the three target K x-ray production cross sections, σ_{Ki}(i=0,1,2), sub-
ject to appropriate initial conditions on the incident ion beam. The
difference between σ_{Ki}(i=1,2) and σ_{KO} provides a means of determing the
K-to-K electron transfer cross sections. Such measurements are similar
to the determination of K-to-K electron transfer cross sections for heavy
ions on gas targets with the exception that the fluorescence yields for
target atoms in the solid do not exhibit a strong dependence on the pro-
jectile charge state.[32]

Another feature of this type of analysis is that by fitting the
target thickness dependences of the averaged target K x-ray production

46

FIGURE 10

Target thickness dependence of measured Al K x-ray production cross sec-
tions for incident 1.0 MeV/amu ions. The solid lines are the results

for a least squares fitting of the 3-component model to the data.

$\overline{\sigma}_{KX} \times 10^{-4}$
(b)

$\rho x (\mu g/cm^2)$

$O^{4+}; Y_0(O) = 1$
$O^{7+}; Y_1(O) = 1$
$O^{8+}; Y_2(O) = 1$

48
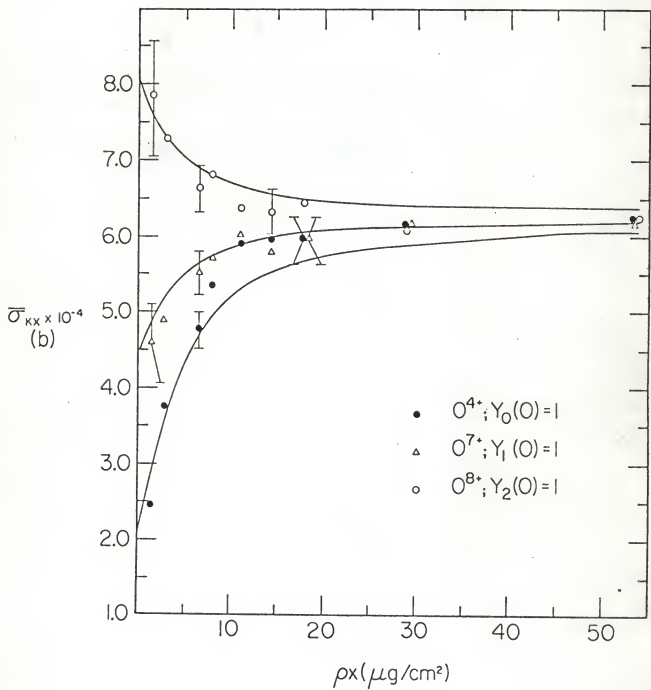
cross sections, $\bar{\sigma}_{Kx}(T)$, with the three-component model[17] the projectile

vacancy production and quenching cross sections σ_{ij}(i=0,1,2, j=0,1,2,

$i{\neq}j$) may be obtained. The target parameters α, β, and σ_{K0} are obtained

from the data by extrapolation of $\bar{\sigma}_{Kx}(T)$ to zero target thickness. The

solid curves in Fig. 10 are the best fit for the three-component model

with α = 2.25, β = 4.0, and $\bar{\sigma}_{K0}$ = 2.0 x 10^4 b. Final fitting parameters

including σ_{ij} are given in Table V. Also included for comparison are

the O electron loss and gain cross sections for thin N_2 and Ar gas target

data from Macdonald and Martin.[33]

The O K-shell vacancy production cross sections σ_{ij}(i<j) for the

solid Al target are ~6-25 times greater than the comparable electrons

loss cross sections for the thin gas targets. Projectiles in both cases

encounter direct Coulomb K-shell ionization through interactions with

target atoms. The difference between the solid and gas target data how-

ever can be qualitatively explained by the effects of a much greater col-

lision frequency in the solid target. Few-electron projectiles which

experience K-shell excitation via collisions in a thin gas target can

decay without charge change and hence the creation of K-shell vacancies

via excitation is not observed in the ion-gas measurement. In contrast

the projectile in a solid which experiences K-shell excitation could un-

dergo another collision before the excited state decays, with the result

that the excited electron is stripped away so that the projectile cannot

fill its K-shell vacancy by decay. In fact target K x-ray production is

sensitive to the number of projectile K-shell vacancies, which is not

necessarily a charge state effect.

The O K-shell quenching cross sections σ_{ij}(i>j) for solids and elec-

tron gain cross sections for gasses are not comparable because the elec-

TABLE V

Parameters from 3-Component Model Calculations of the
Target Thickness Dependences of Al K X-Ray Production
by 1 MeV/amu ^{16}O Ions.

Present Work		Electron Loss and Gain Cross Sections for ^{16}O ions on Gases[a]	
Target Parameters			
σ_{KO}	2×10^{-21}cm^2		
α	2.25		
β	4.0		
Projectile K-shell			
Cross Sections (cm^2)		**Target**	
Vacancy Production		N$_2$	Ar
σ_{01}	2.5×10^{-17}	4×10^{-18}	4×10^{-18}
σ_{12}	1.11×10^{-17}	4×10^{-19}	3×10^{-19}
σ_{02}	5.0×10^{-19}	8×10^{-20}	6×10^{-20}
Quenching			
σ_{21}	8.9×10^{-18}	1.8×10^{-17}	3×10^{-17}
σ_{10}	9.4×10^{-19}	1.5×10^{-17}	2.5×10^{-17}
σ_{20}	5.0×10^{-19}	4.7×10^{-18}	7×10^{-18}

(a) Cross sections taken from the graphical representations of Ref. 33.

tron gain cross sections are total capture cross sections. Captured electron(s) subsequently decay to the ground state, which is allowed under the relatively low collision frequency conditions in the thin gas target. Typically, O electron gain cross sections for the thin gas targets are ~2-25 times greater than $\sigma_{ij}(i>j)$ for solids. In a solid the capture to higher projectile states may be suppressed by the increased collision frequency.

C. K-Shell X-Ray Production and Electron Transfer

Analysis of Al K-shell ionization by O ions has been reported by Laubert and Losonsky (LaL)[34] in the energy range of ~0.06 – 6 MeV/amu using a ~20 ug/cm^2 target. The theoretical cross section calculations of LaL for Al K-shell ionization are based upon the NPSS(CBP) theory,[9] with corrections made for projectile K-shell screening. A screening effect decreases the NPSS(CBP) K-shell ionization cross sections by lowering the polarization correction. Laubert and Losonsky use a constant screening correction over a broad energy range, which is inappropriate by consideration of the equilibrium charge state fractions of O ions moving in a solid shown previously in Fig. 3. They also include contributions to the Al K-shell ionization cross section due to K-to-K electron transfer based upon charge state fractions taken from Marion and Young.[23] However, LaL give no consideration to the O K-shell vacancy configuration as the projectiles move through the target. This is inappropriate in light of the predictions of the three-component model.[17]

Experimental Al K x-ray production cross sections $\sigma_{Ki}(i=0,1,2)$ from this work for incident N, O, and F ions are given in Table VI. The present results for σ_{KO} and $\overline{\sigma}_{Kx}(T=29ug/cm^2)$ for O ions on solid Al targets are compared to PWBA, PSS(CB), PSS(CBP), NPSS(CB), and NPSS(CBP) theoretical calculations in Fig. 11 with $\overline{\omega}_K=0.057$.[25] Target K-shell to projec-

51

TABLE VI

Experimental Al K-Shell X-Ray Production Cross Sections

Determined in the Limit of Zero Target Thickness

σ_{K1} (10^4 b)

E_1/M_1 (MeV/amu)	N→Al(K)			O→Al(K)			F→Al(K)		
	$l=0$	$l=1$	$l=2$	$l=0$	$l=1$	$l=2$	$l=0$	$l=1$	$l=2$
0.6	0.43	0.68	0.91	0.67	1.71	3.33	1.56	6.80	12.7
0.8	0.79	1.28	2.00	1.25	3.55	6.04	3.16	9.76	12.9
1.0	1.23	2.04	3.16	2.00	4.67	8.00	4.21	11.8	22.8
1.2	1.77	2.63	4.32	2.32	5.56	10.2	5.85	15.9	26.9
1.4	1.83	3.12	5.31	3.40	6.80	12.2	7.75	14.7	24.1
1.6	2.39	3.79	5.79	4.43	8.85	14.3	9.23	15.3	23.7
1.8	2.52	4.09	6.05	4.35	8.71	15.3	9.89	18.1	24.5
2.0	2.89	4.91	6.43	5.60	9.45	15.7	9.75	14.8	26.9
2.2	3.03	4.36	6.11	6.15	8.87	14.0	8.72	16.8	26.5

(a) Typical error in these data are taken as ±20%

FIGURE 11

(a) Comparison of experimental Al K x-ray production cross sections, σ_{KO}, and $\bar{\sigma}_{Kx}$ (T = 29 μg/cm^2), for O ions to PWBA, PSS(CB), and PSS(CBP) calculations.

(b) Comparison of experimental Al K x-ray production cross sections, σ_{KO}, and $\bar{\sigma}_{Kx}$ (T = 29 μg/cm^2), for O ions to PWBA, NPSS(CB), and NPSS(CBP) calculations.

Ref. (a) is 34.

$^{16}O \rightarrow Al(K)$

(a)

PWBA
PSS(CB)
PSS(CBP)

(b)

$\sigma_{Ko} \equiv \bar{\sigma}_{KX}(0)$
$\bar{\sigma}_{KX} \, (29\mu g/cm^2)$
σ_{KX}: REF(a)
PWBA
NPSS(CB)
NPSS(CBP)

σ_{KX} (b)

E_1(MeV)
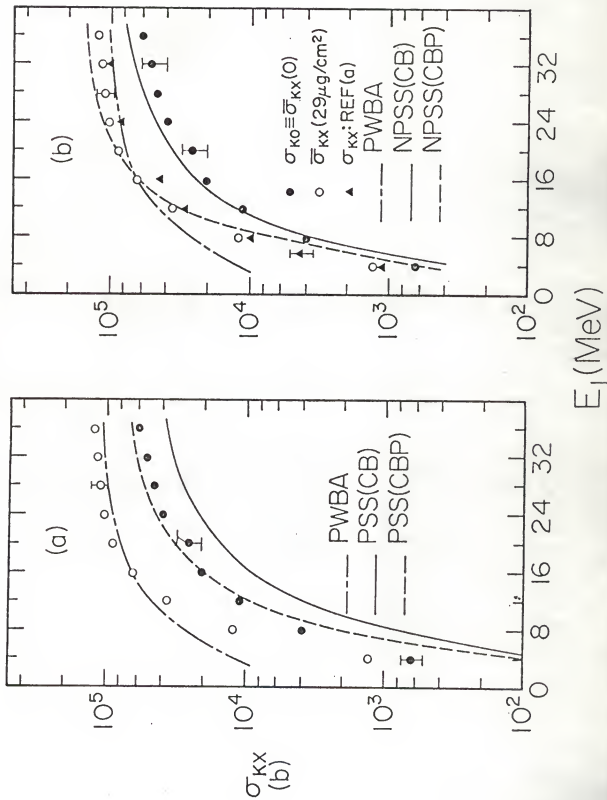
tile L,M,N...-shell (K-to-L,M,N...) electron transfer contributions have not been included in the theoretical calculations given in Figs. 11(a) and 11(b). The target thickness dependence of Fig. 10 shows that $\sigma_{K_X}(T>29\ \mu g/cm^2)$ does not depend upon the number of projectile K-shell vacancies in the incident beam. Furthermore $\sigma_{K_X}(T)$ for a non-zero target thickness is not the single collision cross section and hence the agreement between the NPSS(CBP) calculations and the data as given in Fig. 11(b) for $\sigma_{K_X}(T=29\ \mu g/cm^2)$ is fortuitous.

Target K x-ray production cross sections for projectiles with zero initial K-shell vacancies determined in the limit of zero target thickness, σ_{KO}, are in agreement with both PSS(CBP) and NPSS(CB) calculations, but this comparison does not give a definitive choice between these two theories, which contain different assumptions. The inclusion of the polarization correction indicates that cutoffs in the binding energy correction are not proper, while the use of a cutoff at $r = 1.5\ a_{OK}$ implies that the polarization correction is not required. A systematic comparison of the NPSS(CBP) calculations to experimental σ_{KO} values for N, O, and F ions on Al targets is given in Fig. 12. The NPSS(CBP) calculations systematically overestimate experimental cross sections. In light of this and the unresolved questions as to which of the calculations, PSS (CBP), or NPSS(CB), are appropriate, the K-to-L,M,N... electron transfer contributions to the ionization of the target K-shell are now investigated.

Because ions moving in a solid rapidly lose most electrons outside of the K-shell as shown in Fig. 3, the possibility for K-to-L,M,N... electron transfer exists. Comparison of the PSS(CB) calculations from Table I and scaled OBK electron transfer cross sections from Table III
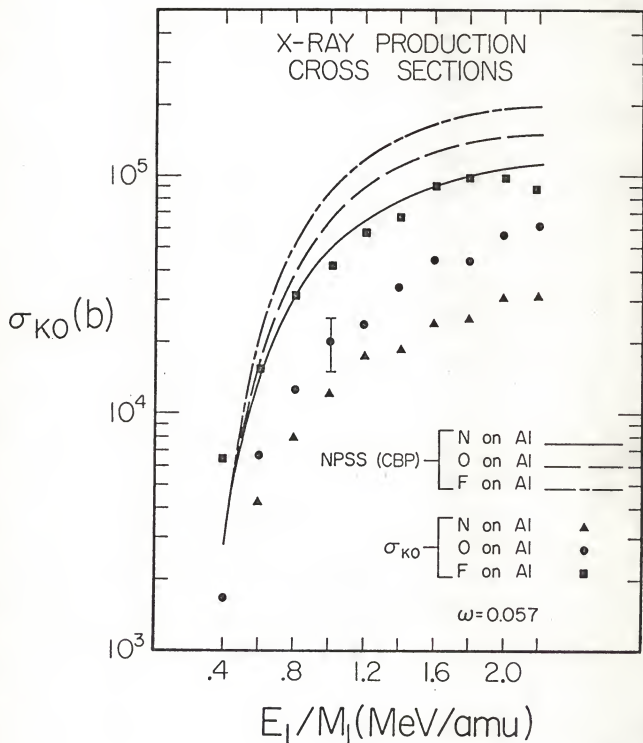
FIGURE 12

Comparison of experimental Al K x-ray production cross sections, σ_{KO}, for N, O, and F ions to NPSS(CBP) calculations.

X-RAY PRODUCTION
CROSS SECTIONS

$\sigma_{KO}(b)$

E_I/M_I(MeV/amu)

NPSS (CBP) — $\begin{bmatrix} \text{N on Al} \\ \text{O on Al} \\ \text{F on Al} \end{bmatrix}$

σ_{KO} — $\begin{bmatrix} \text{N on Al} & \blacktriangle \\ \text{O on Al} & \bullet \\ \text{F on Al} & \blacksquare \end{bmatrix}$

$\omega = 0.057$

shows that the electron transfer contributions are comparable to direct Coulomb ionization processes. Hence the scaled OBK K-to-L,M,N... electron transfer contributions are added to PSS(CB) direct Coulomb ionization calculations to approximate σ_{KO}. The PSS(CB) calculations are utilized because the addition of K-to-L,M,N... electron transfer contributions to either the NPSS(CB) or PSS(CBP) calculations give values of the Al K x-ray production cross sections which systematically overestimate the data for O ions on Al.

Shown in Fig. 13 are the relative contributions of PSS(CB) direct Coulomb ionization and K-to-L,M,N... electron transfer cross sections to the theoretical σ_{KO}^{x} values. The sum of these contributions is given as the solid line in each case. In all cases the K-to-L,M,N... electron transfer contirubtion is a very significant effect, and is the dominant process for F ions on Al. The experimental data for O ions on Al is fit extremely well while the data for N and F ions on Al shows systematic deviations of $\leq 40\%$, with the theory underpredicting and overpredicting the experimentally measured cross sections for F and N projectiles, respectively. These features of the comparison are summarized in Fig. 14.

A systematic deviation such as that observed for N and F ions on Al suggests a fluorescence yield effect. A greater degree of Al L-shell ionization for F ions in comparison to O projectiles is likely. This would result in a greater Al K-shell fluorescence yield in the case of F bombardment. Similarly, less Al L-shell ionization for N bombardment is likely, resulting in a lower Al K-shell fluorescence yield for N projectiles. High resolution x-ray spectroscopic measurements were performed for Al K x-rays from thin Al targets. These measurements show however that Al K-shell fluorescence yields for N, O, and F ion bombardment vary from $\overline{\omega}_K = 0.057$ by at most ~3%. The systematic discrepancy with Z_1 be-

58

FIGURE 13

Comparison of the relative magnitudes of PSS(CB) and scaled OBK K-to-L, M,N... calculations for N, O, and F ions on Al. Also included are the comparisons of experimental σ_{KO} values for N, O, and F ions on Al to the sum of PSS(CB) and OBK K-to-L,M,N... calculations.

K X-RAY PRODUCTION CROSS SECTIONS

F → Al(K)

O → Al(K)

N → Al(K)

σ_{KO} (b)

E_I / M_I (MeV/amu)

σ_{KO} •
σ_{KO}^X ——
$\sigma_{K(DC)}^X$ ———
$\sigma_{K \leftarrow L,M,N, \ldots}^X$ — — —
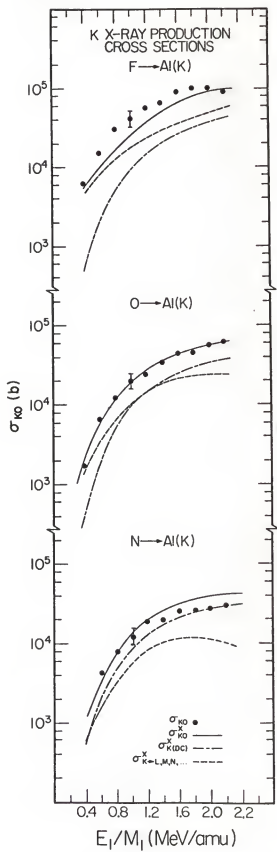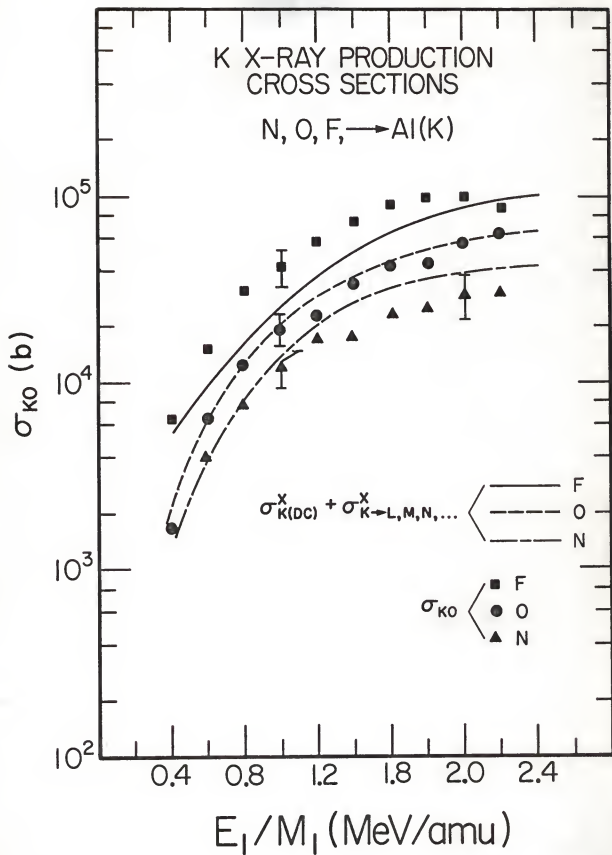
FIGURE 14

Systematic comparison of experimental Al K x-ray production cross sec-
tions, σ_{KO}, for N, O, and F ion bombardment to theoretical σ_{KO}^{x} values,
which are sum of PSS(CB) and scaled OBK K-to-L,M,N... calculations.

K X-RAY PRODUCTION
CROSS SECTIONS

N, O, F, $\longrightarrow$ Al(K)

$\sigma_{K(DC)}^{X} + \sigma_{K \rightarrow L,M,N,...}^{X}$

tween theory and data for σ_{KO} is therefore unresolved at this juncture. Results of the Al K-shell fluorescence yield variation measurements are given in IV D.

Theoretical Al K-shell to projectile K-shell (K-to-K) electron transfer cross sections $\sigma_{iK\to K}(i=1,2)$, expressed as

$$\sigma_{iK\to K(LL)}^{x} = \overline{\omega}_K \sigma_{iK\to K(LL)}$$

are compared to experimental cross sections,

$$\sigma_{iK\to K}^{x} \ (i=1,2) = \sigma_{Ki} - \sigma_{KO}$$

in Figs. 15(a) and 15(b). The $\sigma_{iK\to K(LL)}$ are taken from Table II, and experimental $\sigma_{iK\to K}^{x}$ electron transfer cross sections are given in Table VII. Target K-to-K electron transfer data for O ions on Al is predicted reasonably well by the theory for both hydrogen-like and bare projectiles ($i=1,2$), but experimental $\sigma_{iK\to K}^{x}$ values for N and F ion on Al are somewhat overestimated, and underestimated, respectively.

As previously stated in II B. the ratio $\sigma_{2K\to K}/\sigma_{1K\to K}$ is assumed to be equal to two from statistical considerations. However Fig. 16 demonstrates that the ratio is ~2.3. This may be related to the greater K-shell binding energy of the projectile with two K-shell vacancies in comparison to the one-electron ion. The present data show that the use of a factor of two for $\sigma_{2K\to K}/\sigma_{1K\to K}$ is a reasonable assumption.

D. Fluorescence Yield Variations

High resolution x-ray spectroscopic analysis of Al K x-ray energy spectra for 1.4 MeV/amu N^{+4}, O^{+5}, and F^{+5} ions on thin (~20 ug/cm^2) and thick Al targets gives the average Al L-shell vacancy number, $<\ell> =$ 2.79, 2.93, and 3.09 for N, O, and F ions, respectively. A typical spec-

63

FIGURE 15

(a) Systematic comparison of experimental Al K-to-K electron transfer cross sections for hydrogen-like N, O, and F projectiles, $(\sigma_{1K \to K}^{x} = \sigma_{K1} - \sigma_{K0})$, to theoretical $\sigma_{1K \to K(LL)}^{x}$ calculations.

(b) Systematic comparison of experimental Al K-to-K electron transfer cross sections for bare N, O, and F projectiles $(\sigma_{2K \to K}^{x} = \sigma_{K2} - \sigma_{K0})$, to theoretical $\sigma_{2K \to K(LL)}^{x}$ calculations.

K X-RAY PRODUCTION CROSS SECTIONS

N, O, F, → Al(K) (a)

$\sigma^x_{1K \rightarrow K(LL)}$

$\sigma_{K1} - \sigma_{K0}$

F
O
N

K X-RAY PRODUCTION CROSS SECTIONS

N, O, F, → Al(K) (b)

$\sigma^x_{2K \rightarrow K(LL)}$

$\sigma_{K2} - \sigma_{K0}$

F
O
N

E_I/M_I (MeV/amu)

$\sigma^x_{1K \rightarrow K}$ (b)

$\sigma^x_{2K \rightarrow K}$ (b)

65
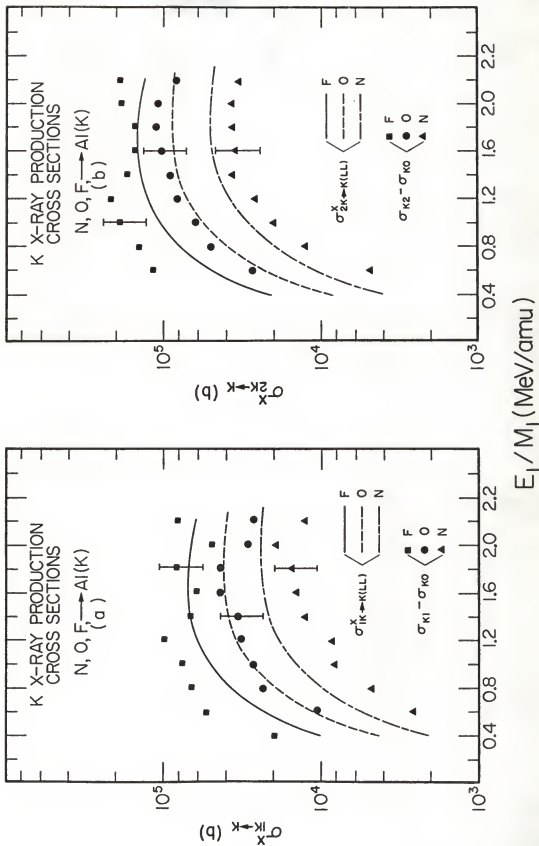
TABLE VII

Experimental Al K-Shell to Projectile K-Shell Electron Transfer

Cross Sections for Bare and Hydrogen-Like Incident Projectiles

$$\sigma_{iK \to K}^{x} (10^{4} b)$$

E_1/M_1 (MeV/amu)	N→Al(K)		O→Al(K)		F→Al(K)	
	$i=1$	$i=2$	$i=1$	$i=2$	$i=1$	$i=2$
0.6	0.26	0.48	1.04	2.67	5.24	11.1
0.8	0.48	1.21	2.30	4.79	6.60	13.8
1.0	0.82	1.94	2.67	6.00	7.60	18.6
1.2	0.85	2.55	3.24	7.87	10.0	21.1
1.4	1.29	3.48	3.40	8.84	6.92	16.4
1.6	1.40	3.40	4.43	9.84	6.11	14.5
1.8	1.57	3.53	4.36	11.0	8.24	14.6
2.0	2.02	3.54	2.95	10.1	5.05	17.2
2.2	1.38	3.08	2.72	7.85	8.08	17.8

(a) Typical errors in these data are taken as ±30%

FIGURE 16

Ratio of experimental Al K-to-K electron transfer cross sections for bare
projectiles (two K-shell vacancies) to experimental K-to-K cross sec-
tions for hydrogen-like projectiles (one K-shell vacancy). The aver-
age is approximately 2.3.

RATIO OF ELECTRON TRANSFER
CROSS SECTIONS FOR
PROJECTILES WITH TWO V.S.
ONE K-SHELL VACANCIES

$N, O, F, \longrightarrow Al(K)$

Y-axis: $\sigma_{K2} - \sigma_{K0} / \sigma_{K1} - \sigma_{K0}$

X-axis: E_I / M_I (MeV/amu)

Legend:
■ F
● O
▲ N
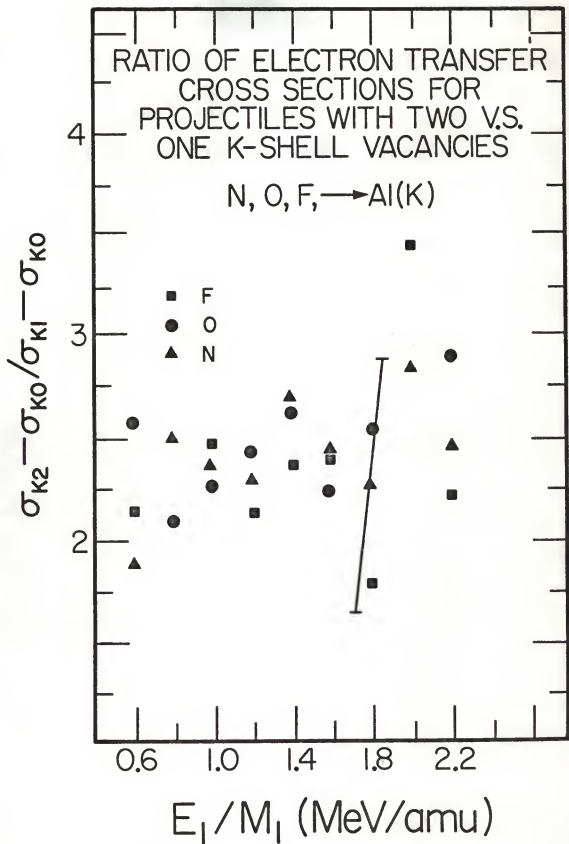
trum for 1.4 MeV/amu N ions on Al is shown in Fig. 17. Comparisons of target K x-ray spectra for thin and thick targets show that the spectral distribution is the same in both cases. The Al K-shell fluorescence yields for the three cases were not significantly different, as $\overline{\omega}_K$ = 0.056, 0.057, and 0.059 for N, O, and F ions, respectively.

The weighted average

$$1/\overline{\omega}_K = \sum_{\ell=0}^{\ell max} f_\ell/\omega_\ell$$

may be used to calculate $\overline{\omega}_K$ from the high resolution data. Here f_ℓ is the fraction of target K x rays that come from atoms with ℓ L-shell vacancies, and the ω_ℓ are the target K-shell configuration fluorescence yields as scaled from the results of Doyle et al.[26] for Si ions on a He gas target. The f_ℓ are obtained from the spectra, as the ratio of the intensity of the ℓth peak to the total intensity. Values of f_ℓ and ω_ℓ are given in Table VIII.

FIGURE 17

High resolution Al K x-ray energy spectra for 1.4 MeV/amu N^{+4} bombardment a thick Al target.

Al(K) X-RAY PRODUCTION
1.4 MeV/amu N^{+4} ⟶ Al (THICK TARGET)
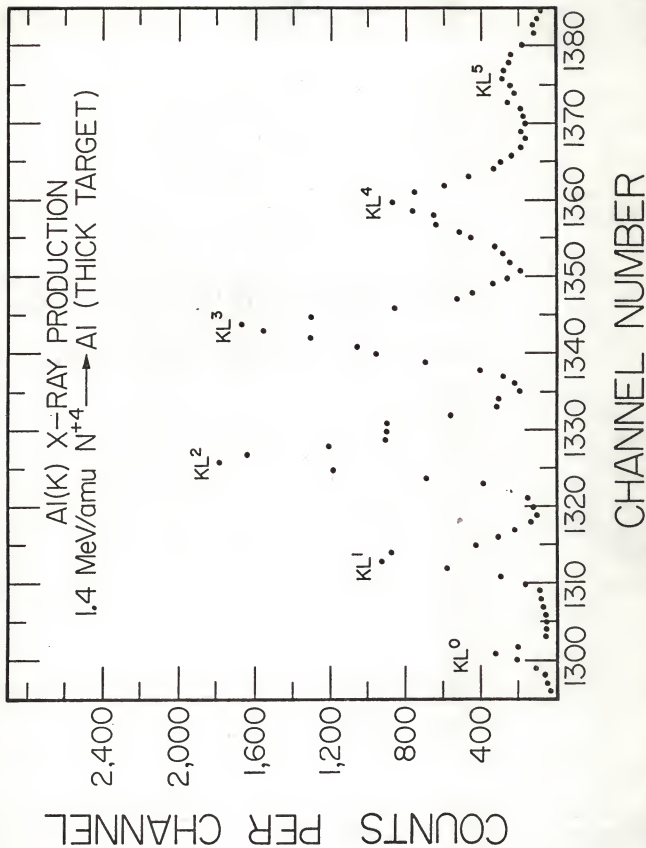
TABLE VIII

Experimental Al L-Shell Vacancy Fractions

for 1.4 MeV/amu N, O, F→Al(K)

and

Si(K) Configuration Fluorescence Yields[a]

	N→Al	O→Al	F→Al
f_0	0.026	0.024	0.022
f_1	0.109	0.087	0.076
f_2	0.281	0.257	0.210
f_3	0.306	0.308	0.332
f_4	0.192	0.213	0.216
f_5	0.086	0.110	0.140
f_6	0.0	0.0	0.004
f_7	0.0	0.0	0.0
	$\langle \ell \rangle = 2.79$	$\langle \ell \rangle = 2.93$	$\langle \ell \rangle = 3.08$

ω_0	0.044
ω_1	0.054
ω_2	0.063
ω_3	0.068
ω_4	0.079
ω_5	0.089
ω_6	0.121

(a) Values taken from Ref. 26.

V. SUMMARY

Target K x-ray production for heavy ions where $Z_1/Z_2 \sim 0.6$ is shown to depend strongly on the number of projectile K-shell vacancies brought into collisions, but is independent of the L-shell configuration of the projectile prior to its entering the target. Furthermore, the target K x-ray production cross section for projectiles incident with i K-shell vacancies (i=0,1,2) show very pronounced target thickness effects which make the analysis of target K x-ray production for non-zero thickness targets an extremely involved process. By using the target K x-ray production cross sections for projectiles with i K-shell vacancies (i=0,1,2) under single collision conditions, i.e. taken in the limit of zero target thickness, σ_{Ki} (i=0,1,2) are obtained. The projectile K-shell vacancy production and quenching cross section, σ_{ij} (i=0,1,2, j=0,1,2, i≠j), are obtained by fitting the target thickness dependent target K x-ray production cross sections with the three-component model.[17] Heavy ion K-shell vacancy production cross sections in a solid are significantly greater than comparable electron loss cross sections in thin gas targets.[33] Projectile vacancy quenching cross sections in the solid however are significantly smaller than electron gain cross sections in the thin gas. The greater collision frequency in the solid may be a contributing factor to these differences, though this general area of projectile vacancy production and quenching processes is one that should be systematically investigated further.

The indpendence of target K x-ray production on the L-shell configuration of the projectile prior to its entering the target demonstrates that solid target K-shell fluorescence yields are not strongly dependent upon projectile charge state. Furthermore, high resolution target K

x-ray energy spectroscopic measurements show that both thick and thin solid target K-shell fluorescence yields are independent of incident projectile charge state. Therefore, the study of thin solid target K x-ray production data in the limit of zero target thickness provides for a more straightforward evaluation of target K-shell ionization processes than does thin gas target data insofar as the fluorescence yield is concerned.

A model for target K-shell ionization by projectiles with zero K-shell vacancies, σ_{KO}, is constructed using the assumption that the projectile L-shell essentially contains no electrons immediately after entering the target. By adding scaled OBK target K-shell to projectile L,M,N...-shell electron transfer cross section contributions to PSS(CB) direct Coulomb ionization calculations, the experimental σ_{KO} values for N, O, and F ions on Al are approximated reasonably well. There are however systematic discrepancies in the cases of N and F on Al that are not resolved on the basis of fluorescence yield variations and require additional study.

Theoretical PSS(CBP), NPSS(CB), and NPSS(CBP) calculations significantly overestimate experimental σ_{KO} values when electron transfer contributions are included. In light of this, it is apparent that target K-shell polarization and radial cutoffs in the K-shell binding energy correction should not be utilized where the K-shell ionization is effected by heavy ions, although both PSS(CB) and NPSS(CBP) calculations are in good agreement with experimental K-shell ionization of a variety of targets by light ions,[9] where electron transfer contributions to the ionization process can be neglected and the corrections contained in these direct ionization calculations are small.

74

The target K-shell to projectile K-shell (K-to-K) electron transfer cross sections for projectiles with i K-shell vacancies, σ_{iK+K}^{x} $(i=1,2)$, are expressed in terms of the difference $\sigma_{Ki} - \sigma_{K0}$, $(i=1,2)$. The measured K-to-K electron transfer cross sections of the present work are in good agreement with the electron transfer calculations of Lapicki and Losonsky. It is assumed that $\sigma_{2K \to K} / \sigma_{1K \to K} = 2$, but present results suggest that the ratio is ≈ 2.3, which may be related to the difference in K-shell binding energies of the one-electron and bare projectiles. The experimental $\sigma_{1K \to K}^{x}$ values for O ions on Al are predicted well by the theory but for N and F ions on Al the data show systematic discrepancies similar to those for the comparison of experimental σ_{K0}'s to theory.

The analysis of target K x rays produced via heavy ion bombardment on a series of thin solid targets of varying thickness yields a wealth of information that is not available by other experimental techniques. Information concerning both projectile and target K-shell vacancy production and projectile K-shell vacancy quenching can be obtained. This work shows that meaningful measurements of fundamental ionization and electron transfer processes can be performed in solids. The range of atomic numbers for the collision partners is thus expanded over that available for ion-gas target systems to allow broader systematic studies of inner-shell ionization in collisions.

APPENDIX

Sample calculations for NPSS(CBP) direct Coulomb ionization, Lapicki and Losonsky K-to-K electron transfer, and OBK K-to-L electron transfer cross sections for 1.0 MeV/amu N ions on Al are given below. As referred to in II A., all of the cross section calculations in both PSS and NPSS theory may be obtained from appropriate considerations of the elements used in the NPSS(CBP) calculation. Also, only the OBK K-to-L electron transfer cross section is calculated, as the K-to-M,N... calculations follow closely.

The primary quantities for the NPSS(CBP) calculation are:

$$\theta_K = \hbar\omega_{2K}/Z_{2K}^2 \; 13.6 \text{ eV} = 1560 \text{ eV}/(13-0.3)^2 13.6 \text{ eV} = 0.711$$

$$\eta_K = (E_1/M_1)/1836 \; Z_{2K}^2 13.6 \text{ eV} = 0.248,$$

$$\xi_K = 2\eta_K^{1/2}/\theta_K = 1.41.$$

Using $c_K = 1.5$ gives $g_K(1.41, 0.711) = 0.209$ by interpolation from Table V, Ref. 9. Also $I(c_K/\xi_K) = 0.19$ by interpolation from Table IV from Ref. 9. From these values, the value of ζ_K is calculated as

$$\zeta_K = 1 + (2Z_1/\theta_K Z_{2K})(g(\xi_K, \; c_K) - h(\xi_K, \; c_K)) = 1.03$$

$$\text{where } h(\xi_K, \; c_K) = (2/\theta_K \xi_K^3)I(c_K/\xi_K),$$

so that $\zeta_K \theta_K = 0.73$. The argument of the function F_K then becomes

$$\eta_K/(\zeta_K \theta_K)^2 = 0.465, \text{ so } F_K(0.465) = 0.474 \text{ from Ref. 10.}$$

In this example,

$$\sigma_{OK} = 8\pi a_o^2 (Z_1/Z_{2K}^2)^2 = 1.33 \times 10^6 b \quad .$$

76

The Coulomb deflection correction is

$$C_K(\pi d q_o \zeta_K) \cong 1,$$

so the direct Coulomb ionization cross section then is

$$\sigma_{K(DC)(NPSS(CBP))} \cong C_K(\sigma_{OK}/\tau_K \theta_K) F_K(0.465)$$

$$\cong 1.33 \times 10^6 b \ (0.474/0.73)$$

$$\cong 8.6 \times 10^5 b \ .$$

The primary quantities for the Lapicki and Losonsky K-to-K electron transfer calculation are:

$$\theta_K = 0.711,$$

$$v_1 = 6.4 \text{ (in atomic units)} \ ,$$

$$v_{2K} = Z_{2K} = 12.7 \ ,$$

$$v_{1K} = Z_1 = 7 \ ,$$

$$M_1 = 14 \times 1836 \ ,$$

$$M_2 = 27 \times 1836.$$

This allows for the calculation of:

$$d = (Z_1 Z_2/v_1^2)(1/M_1 + 1/M_2) = 1.31 \times 10^{-4} \ ,$$

$$d_{KK} = d(1 - (v_{2K}^2 \theta_K - v_{1K}^2)/v_1^2 M)^{-1/2} \ ,$$
$$\text{with } 1/M = 1/M_1 + 1/M_2 \ ,$$

$$d_{KK} \cong d = 1.31 \times 10^{-4} \text{ since } (v_{2K}^2 \theta_K - v_{1K}^2)/v_1^2 M \ll 1 \ ,$$

$$q_{KK} (\theta_K) = (v_{2K}^2 \theta_K - v_{1K}^2)/2v_1 + v_1/2 = 8.35 \ ,$$

$$\beta^{1/2} = (q_{KK}^2 + v_{1K}^2)^{1/2} = 10.9,$$

$$v_{2K}/\beta^{1/2} = 1.17,$$

$$g_K(1.17) = (1 + 5(1.17) + 7.14(1.37) + 4.27(1.60) + 0.95(1.87))/$$
$$(1 + 1.17)^5 = 0.525,$$

$$\varepsilon_K = 1 + (2Z_1/Z_{2K}\theta_K)g_K(v_{2K}/\beta^{1/2}) = 0.91,$$

$$\varepsilon_K^{1/2} = 0.954,$$

$$\varepsilon_K\theta_K = 0.68,$$

$$q_{KK}(\varepsilon_K\theta_K) = 7.9,$$

$$\exp-(\pi d_{KK} q_{KK}(\varepsilon_K\theta_K)) \cong 1.$$

The cross section in the high velocity limit $\sigma_{2K\to K}(\geq)$, is

$$(1/3)\sigma_{2K\to K(OBK)}(\theta_K) = (1/3)a_o^2(2^9/5v_1^2)\frac{(v_{1K}v_{2K})^5}{(v_{1K}^2+(v_1^2+v_{2K}^2-v_{1K}^2)^2/4v_1^2)^5}$$

$$= 7.7 \times 10^5 b.$$

In the low velocity limit $\sigma_{2K\to K}(<<) = \exp-(\pi d_{KK} q_{KK}(\varepsilon_K\theta_K))\sigma_{2K\to K}(\varepsilon_K\theta_K)$

$$\cong \pi a_o^2(2^9/5v_1^2)\frac{(v_{1K}\varepsilon_K^{1/2}v_{2K})^5}{(v_{1K}^2+(v_1^2+\varepsilon_Kv_{2K}^2-v_{1K}^2)/4v_1^2)^5}$$

$$\cong 12.3 \times 10^5 b$$

where $v_{2K}\to\varepsilon_K^{1/2}v_{2K}$ when $\theta_K\to\varepsilon_K\theta_K$.

The interpolation formula yields the K-to-K electron transfer cross section

$$\sigma_{2K \to K(LL)} = \frac{\sigma_{2K \to K}(\geq) \sigma_{2K \to K}(<<)}{(2/3)\sigma_{2K \to K}(<<) + \sigma_{2K \to K}(\geq)}$$

$$\cong 5.2 \times 10^5 b \quad .$$

The primary quantities for the Nikolaev OBK K-to-L electron transfer calculation are:

$$V = v_1/v_{2K} = 0.592,$$

$$\eta_n = (Z_1^2 \ 13.6 \ eV/n_1^2 \hbar \omega_{2K})^{1/2} = 0.327,$$

therefore $\gamma = 4V^{-2}(1 + 2(1+\eta_n)/V^2 + (1-\eta_n^2)^2/V^4)^{-1} = 0.765$. The K-to-L electron transfer cross expression

$$\sigma_{K \to L(OBK)} = \pi a_o^2 4 (2^9/5) (v_o/V)^2 \gamma^5 \eta_n^5$$

is then calculated in a straightforward manner, using $V_o = e^2/\hbar$ which gives

$$\sigma_{K \to L(OBK)} = 1.2 \times 10^6 b \quad .$$

REFERENCES

1.   J. Chadwick, Phil. Mag. $\underline{24}$, 594 (1912).

2.   Patrick Richard, <u>Atomic Inner-Shell Processes</u>, Bernd Crasemann, Ed. (Academic Press, New York, 1975), Vol. 1, p. 73, and references therein.

3.   J. D. Garcia, E. Gerjuoy, and J. E. Welker, Phys. Rev. $\underline{165}$, 66 (1968).

4.   J. Bang and J. M. Hansteen, K. Dan. Vidensk. Selsk. Mat. - Fys. Medd. $\underline{31}$, No. 13 (1959).

5.   E. Merzbacher and H. W. Lewis, <u>Handbuch der Physik</u>, S. Flugge, Ed. (Springer-Verlag, Berlin, 1958), Vol. 34, p. 166.

6.   W. Brandt, R. Laubert, and I. Sellin, Phys. Rev. $\underline{151}$, 56 (1966).

7.   G. Basbas, W. Brandt, and R. Laubert, Phys. Rev. A$\underline{7}$, 983 (1973).

8.   K. W. Hill and E. Merzbacher, Phys. Rev. A$\underline{9}$, 156 (1974).

9.   G. Basbas, W. Brandt, and R. Laubert, Phys. Rev. A$\underline{17}$, 1655 (1978), and private communication.

10.   R. Rice, G. Basbas, and F. McDaniel, At. Data Nucl. Data Tables (to be published).

11.   J. R. Oppenheimer, Phys. Rev. $\underline{31}$, 349, (1928).

12.   H. C. Brinkman and H. A. Kramers, Proc. Acad. Sci. (Amsterdam), $\underline{33}$, 973 (1930).

13.   V. S. Nikolaev, Soviet Phys.-JETP $\underline{24}$, 847 (1967).

14.   G. Lapicki and W. Losonsky, Phys. Rev. A$\underline{15}$, 896 (1977).

15.   J. A. Guffey, M. Sc. thesis (Kansas State University, 1974) (unpublished).

16.   Tom J. Gray, Patrick Richard, K. A. Jamison, J. M. Hall and R. K. Gardner, Phys. Rev. A$\underline{14}$, 1333 (1976).

17. R. K. Gardner, Tom J. Gray, Patrick Richard, Carl Schmiedekamp, K. A. Jamison and J. M. Hall, Phys. Rev. A$\underline{15}$, 2002 (1977).

18. F. Hopkins, Phys. Rev. Lett. $\underline{35}$, 270 (1975).

19. Forrest Hopkins, Jonathan Sokolov and Andrew Little, Phys. Rev. A$\underline{15}$, 588 (1977).

20. K. O. Groeneveld, B. Kolb, J. Schader and K. D. Sevier, Z. Phys. A$\underline{277}$, 13 (1976).

21. F. D. McDaniel, J. L. Duggan, George Basbas, P. D. Miller and Grzegorz Lapicki, Phys. Rev. A$\underline{16}$, 1375 (1977).

22. A. M. Halpern and J. Law, Phys. Rev. Letts. $\underline{31}$, 4 (1973).

23. J. B. Marion and F. C. Young, Nuclear Reaction Analysis, (North-Holland, Amsterdam, 1968), p. 43.

24. H. Tawara et. al. (to be published).

25. Forrest Hopkins, D. O. Elliott, C. P. Bhalla and Patrick Richard, Phys. Rev. A$\underline{8}$, 2952 (1973).

26. B., L. Doyle, U. Schiebel, J. R. Macdonald and L. D. Ellsworth, Phys. Rev. A$\underline{17}$, 523 (1978).

27. Ref. 23, p. 154.

28. R. Marrus, Current Topics in Physics - Beam Foil Spectroscopy, S. Bashkin, Ed. (Springer-Verlag, Berlin, 1976) Vol. 1, p. 209.

29. Schnopper et al., Phys. Rev. Lett. $\underline{29}$, 898, (1972).

30. Ref. 23, p. 147.

31. L. C. Northcliff and R. F. Schilling, Nuclear Data Tables $\underline{7}$, 2681 (1970).

32. P. Richard et al., private communication.

33. J. R. Macdonald and F. W. Martin, Phys. Rev. A$\underline{4}$, 1965 (1971).

34. Roman Laubert and William Losonsky, Phys. Rev. A$\underline{14}$, 2043 (1976).

35. H. Tawara, Y. Hachiya, K. Ishii and S. Morita, Phys. Rev. A$\underline{13}$, 572 (1976).

ALUMINUM K X-RAY PRODUCTION AND ELECTRON

TRANSFER CROSS SECTIONS FOR OXYGEN, NITROGEN, AND FLUORINE

IONS FROM 0.6 TO 2.2 MEV/AMU

by

Glenn S. Gealy

B. A., Hastings College, 1974

AN ABSTRACT OF A MASTER'S THESIS

submitted in partial fulfillment of the

requirements for the degree

MASTER OF SCIENCE

Department of Physics

Kansas State University

Manhattan, Kansas 66506

1978

ABSTRACT

Thin solid Al targets ranging in thickness from 1-50 ug/cm^2 were bombarded by ^{14}N, ^{16}O, and ^{19}F ions with incident energies from 0.6 to 2.2 MeV/amu. The effects of target thickness on the measured Al K x-ray yield for O ions incident with zero, one, and two initial K-shell vacancies were determined, and the O K-shell vacancy production and quenching cross sections deduced. Comparisons of the data for Al K x-ray production in vanishingly thin and 29 ug/cm^2 targets for O ions incident without an initial K-shell vacancy are made to Perturbed Stationary State calculations (PSS). The PSS calculations contain corrections for Coulomb deflection and binding energy (PSS(CB)) and Coulomb deflection, binding energy and polarization (PSS(CBP)). Further two different PSS calculation procedures are employed: (1) calculations without radial cutoffs employed in the binding energy correction contribution (PSS) and (2) calculations with radial cutoffs employed in the binding energy correction (NPSS). The PSS(CBP) and NPSS(CB) calculations both agree with the measured Al K x-ray production cross sections for data taken in the limit of a vanishingly thin target. The NPSS(CBP) calculations agree with the data taken for a 29 ug/cm^2 Al target. The latter agreement is fortuitous as the observed increase in the measured target x-ray yield for the 29 ug/cm^2 target in comparison to the yield extracted as $\rho x \to 0$ at each bombarding energy is due to target K-shell to projectile K-shell (K-to-K) electron transfer. The zero target thickness Al K x-ray production cross section for N, O, and F ions is approximated as the sum of PSS(CB) K-shell ionization and scaled OBK Al K-shell to projectile L,M,N...-shell electron transfer calculations. The Al K-to-K electron

transfer cross sections for bare and hydrogen-like N, O, and F ions were extracted from the target production data for incident ions with 0, 1, and 2 initial K-shell vacancies. These measurements are compared to the K-to-K electron transfer calculations of Lapicki and Losonsky.